iScience

CellPress
OPEN ACCESS

Article

Adipose-specific overexpression of human AGPAT2 in mice causes increased adiposity and mild hepatic dysfunction

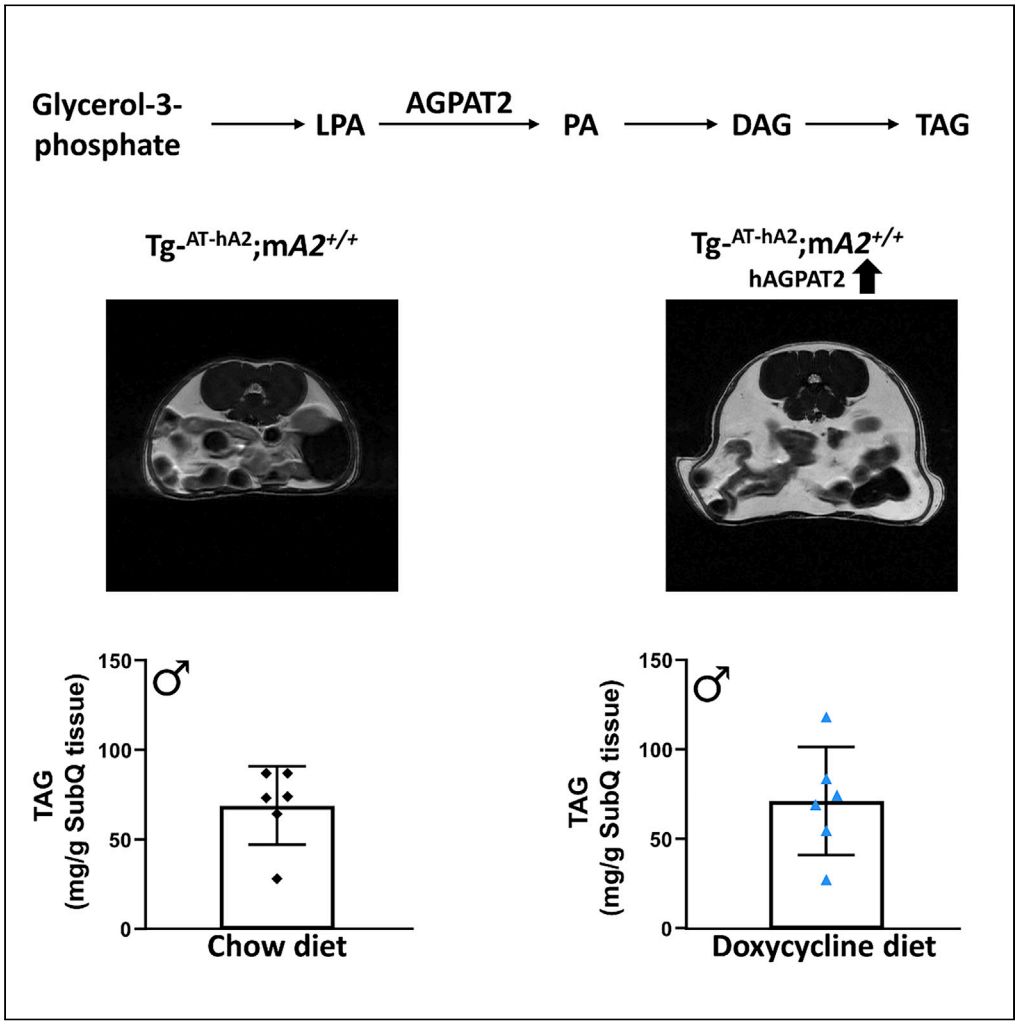

Anil K. Agarwal, Katie Tunison, Goncalo Vale, Jeffrey G. McDonald, Xilong Li, Jay D. Horton, Abhimanyu Garg

anil.agarwal@utsouthwestern.edu

Highlights

Overexpression of hAgpat2 in mice increased adiposity with mild liver dysfunction

The increased adipose tissue mass did not increase adipose tissue TAG

A modest increase in adipose mass did show mild liver dysfunction

Increased h*Agpat2* expression shows mild adipose tissue hyperplasia

Agarwal et al., iScience *27*, 108653
January 19, 2024
https://doi.org/10.1016/j.isci.2023.108653

iScience

CellPress
OPEN ACCESS

Article

Adipose-specific overexpression of human AGPAT2 in mice causes increased adiposity and mild hepatic dysfunction

Anil K. Agarwal,[1,2,5,*] Katie Tunison,[1,2] Goncalo Vale,[2,3] Jeffrey G. McDonald,[2,3] Xilong Li,[4] Jay D. Horton,[2,3] and Abhimanyu Garg[1,2]

SUMMARY

AGPAT2, a critical enzyme involved in the biosynthesis of phospholipids and triacylglycerol (TAG), is highly expressed in adipose tissue (AT). Whether overexpression of AGPAT2 in AT will result in increased TAG synthesis (obesity) and its metabolic complications remains unknown. We overexpressed human *AGPAT2* specifically in AT using the adiponectin promoter and report increased mass of subcutaneous, gonadal, and brown AT in wild-type mice. Unexpectedly, overexpression of h*AGPAT2* did not change the pattern of phospholipid or TAG concentration of the AT depots. Although there is an increase in liver weight, plasma aspartate aminotransferase, and plasma insulin at various time points of the study, it did not result in significant liver dysfunction. Despite increased adiposity in the Tg-$^{AT\text{-}hAGPAT2;}$m*Agpat2*$^{+/+}$ mice, there was no significant increase in TAG concentration of AT. Therefore, this study suggests a role of AGPAT2 in the generation of AT, but not for adipocyte TAG synthesis.

INTRODUCTION

AGPAT2 (1-acylglycerol-3-phosphate O-acyltransferase 2) is an enzyme that converts lysophosphatidic acid (LPA) to phosphatidic acid (PA).[1] PA is a substrate for several phospholipids, including phosphatidylcholine (PC), phosphatidylethanolamine (PE), and phosphatidylinositol (PI), and is also a substrate for diacylglycerol (DAG) and triacylglycerol (TAG) biosynthesis.[1]

Ever since we discovered that the loss of functional *AGPAT2* leads to the loss of adipose tissue (AT), resulting in the development of congenital generalized lipodystrophy (CGL) Type 1 (CGL1) phenotype in both humans[2] and mice,[3] an argument has been put forward that adipocytes are present in CGL1 patients and recombinant animals but they are unable to biosynthesize and accumulate TAG in the adipocytes. The other argument is that both humans and mice with CGL1 lack adipocytes *per se*. To investigate these arguments, we generated a transgenic mouse model expressing human *AGPAT2* specifically in AT, driven by the adiponectin promoter, and regulated by doxycycline (dox)[4] (Figures S1A and S1B). Using this strategy, we observed the regeneration of AT, albeit at a reduced quantity (~30–50%) compared to wild-type mice of similar age. Additionally, when the expression of *AGPAT2* is turned off by removing doxycycline (dox) from the animal's diet, within 8 weeks there is undetectable AT in the mice. We also show in the same study that when stromal vascular fraction cells from the generated AT are differentiated *ex vivo*, they only differentiated in the presence of dox, which turns on the expression of *hAGPAT2*, further confirming the *in vivo* observation.[4]

Whether overexpression of AGPAT2 in adipose tissue (AT) will result in increased AT mass (obesity) and its metabolic complications remains unknown. Therefore, we generated mice (wild type for mouse *Agpat2*) specifically expressing human *AGPAT2* (h*AGPAT2*) regulated by dox in AT. These mice express h*AGPAT2* in the background of normal expression of mouse *Agpat2*. In this context, we consider these mice as overexpressing *AGPAT2* in AT only, resulting in a murine model to study its role in AT. When turned on (by feeding dox diet), the increased expression of h*AGPAT2* should increase the synthesis of TAG over and above the normal TAG synthesis. Alternatively, if its role in TAG synthesis is minimal, we expect the synthesis of TAG in these mice to increase only slightly, or remain unchanged compared to those WT mice fed a chow diet (i.e., mice not overexpressing h*AGPAT2*). In this study, we set out to clarify the issue of whether AGPAT2 increases TAG synthesis in the adipocytes. The findings described here are part of a larger study where we show the regeneration of AT in *Agpat2*$^{-/-}$ mice[4] and the resulting amelioration of hepatic steatosis in Tg-$^{AT\text{-}hA2}$;mA2$^{-/-}$ mice with regenerated AT. The findings will be presented later in the same journal or elsewhere.

[1]Section of Nutrition and Metabolic Diseases, Division of Endocrinology, Department of Internal Medicine, UT Southwestern Medical Center, Dallas, TX 75390, USA
[2]Center for Human Nutrition, UT Southwestern Medical Center, Dallas, TX 75390, USA
[3]Department of Molecular Genetics, UT Southwestern Medical Center, Dallas, TX 75390, USA
[4]Peter O'Donnell Jr. School of Public Health, UT Southwestern Medical Center, Dallas, TX 75390, USA
[5]Lead contact
*Correspondence: anil.agarwal@utsouthwestern.edu
https://doi.org/10.1016/j.isci.2023.108653

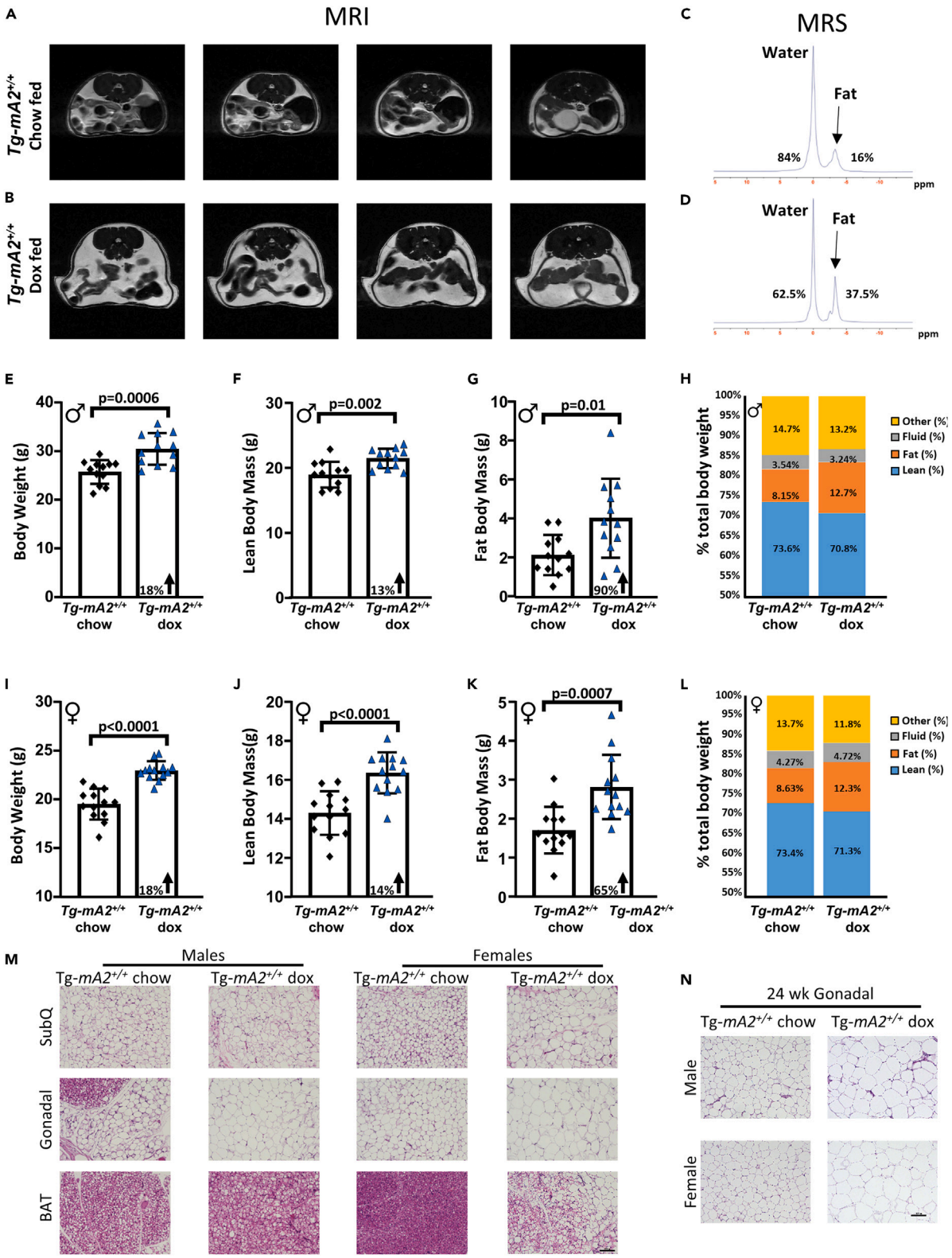

Figure 1. Overexpressing human *AGPAT2* transgene in Tg-$^{AT\text{-}hA2}$;*mA2*$^{+/+}$ mice results in increased body weight and fat mass

(A) Magnetic resonance imaging (MRI) of a 14 week old male chow-fed Tg-$^{AT\text{-}hA2}$;*mA2*$^{+/+}$ mouse. Shown are representative axial slices of the abdomen taken at regular intervals.

Figure 1. *Continued*

(B) MRI of 14 week old male doxycycline (dox)-fed Tg-$^{AT\text{-}hA2}$;*mA2*$^{+/+}$ mouse. Increased fat mass can be observed in this mouse compared to the chow-fed Tg-$^{AT\text{-}hA2}$;*mA2*$^{+/+}$ mouse in panel A (fat is white color).

(C and D) Quantitation of fat mass by magnetic resonance spectrometry (MRS) shows the increased fat content in the (D) dox-fed Tg-$^{AT\text{-}hA2}$;*mA2*$^{+/+}$ mouse compared to the (C) chow-fed Tg-$^{AT\text{-}hA2}$;*mA2*$^{+/+}$ mouse.

(E and I) Body composition of Tg-$^{AT\text{-}hA2}$;*mA2*$^{+/+}$ mice as assessed by nuclear magnetic resonance: total body weight of (E) males and (I) females. A significant increase in body weight of dox-fed Tg-$^{AT\text{-}hA2}$;*mA2*$^{+/+}$ mice is noted in both sexes.

(F and J) Dox-fed Tg-$^{AT\text{-}hA2}$;*mA2*$^{+/+}$ mice also show increased lean mass in (F) males and (J) females.

(G and K) The fat mass is also significantly increased in dox-fed Tg-$^{AT\text{-}hA2}$;*mA2*$^{+/+}$ mice in both (G) males and (K) females.

(H and L) When fat is expressed as a percent of total body weight, both (H) male and (L) female dox-fed Tg-$^{AT\text{-}hA2}$;*mA2*$^{+/+}$ mice show a slight increased percent fat compared to chow-fed Tg-$^{AT\text{-}hA2}$;*mA2*$^{+/+}$ mice. About 12–15% of the total body weight is composed of bone, fur, claws, and so forth (marked as "other"). The percent increase of dox-fed vs. chow-fed Tg-$^{AT\text{-}hA2}$;*mA2*$^{+/+}$ mice is shown inside the bar. The data are represented as mean ± SD. Individual data points are shown within the bars. P-values were calculated using the Student's *t* test.

(M-N) Hematoxylin and eosin-stained histological images of white and brown adipose tissue (AT) from (M) 12 week old Tg-$^{AT\text{-}hA2}$;*mA2*$^{+/+}$ mice of both sexes, either maintained on chow or dox diet, and (N) gonadal AT at 24 weeks. 20x images. Scale bars are 100 μm. Tg-$^{AT\text{-}hA2}$;*mA2*$^{+/+}$ abbreviated to Tg-*mA2*$^{+/+}$. See also Figure S1.

RESULTS

Generation and initial characterization of transgenic Tg-$^{AT\text{-}hA2}$;mA2$^{+/+}$ mouse model

The generation and initial characterization of these transgenic mice is described in a recently published article.[4] For AT-specific re-expression of hAGPAT2 in mice, we required generation and multiple crossing of three mouse lines: (1) a mouse strain expressing *hAGPAT2* driven by TRE-tight/PminCMV promoter system (see[4] for detailed experimental generation and characterization of mice); (2) a mouse strain expressing rtTA driven by an adiponectin promoter[5] and (3) an *Agpat2*$^{+/-}$ mouse strain.[3] Our mating strategy and generation of experimental mice is shown in Figure S1D. In this strategy, we obtained wild-type Tg-h*AGPAT2, Adipo*-rtTA, m*Agpat2*$^{+/+}$mice, which, when fed a dox-diet, will express hAGPAT2, essentially generating an over-expressing AGPAT2 mouse model. The mouse strain used in this study, Tg-h*AGPAT2, Adipo*-rtTA, m*Agpat2*$^{+/+}$, is abbreviated hereafter as Tg-$^{AT\text{-}hA2}$;*mA2*$^{+/+}$. This nomenclature/abbreviation denotes transgenic mice expressing h*AGPAT2* in a wild-type genetic background. The compound transgenic line we generated (Tg-$^{AT\text{-}hA2}$;mA2$^{+/-}$) is on a mixed genetic background of C57Bl/6NTac and 129S6/SvEvTac. Likewise, the wild-type (B6129F1; abbreviated B6/129)) mice used to ascertain the effect of the doxycycline diet are also on a mixed genetic background (C57Bl/6NTac and 129S6/SvEvTac). We performed a direct genetic comparison between the compound Tg-$^{AT\text{-}hA2}$;mA2$^{+/-}$ strain versus controls (B6/129) to determine the strain heterozygosity. The data generated is from a Mouse Genome Scanning Panel based on approximately 1113 SNPs (curated by Taconic Biosciences) and selected specifically to highlight differences between inbred mouse strains. Additionally, B6/129 mice have been used primarily as a control for studies involving the use of targeted gene-mutated mice on a mixed background originating from 129 ES cell-based chimeras that were subsequently mated to C57BL/6 mice. While they are not genetically identical to these mixed background targeted mutation models, they approximate, in a consistent manner, the genetic mix that may be present in such models (https://www.taconic.com/mouse-model/b6129f1). The data for the chow-fed Tg-$^{AT\text{-}hA2}$;*mA2*$^{+/+}$ mice are the same as shown in[4] and those pertaining to hepatic steatosis in these mice to be published in this journal or elsewhere, as the experiments for all the three studies were conducted concurrently.

Measurement of body composition by magnetic resonance imaging, nuclear magnetic resonance, magnetic resonance spectrometry, and adipose histology

The presence of AT was evaluated in chow-fed and dox-fed Tg-$^{AT\text{-}hA2;}$mA2$^{+/+}$ mice by non-invasive magnetic resonance imaging (MRI) in one male mouse per condition at 14 weeks. There was an increase in the presence of AT mass in dox-fed mice compared to those on a chow diet (Figures 1A and 1B). Additionally, AT was quantified by magnetic resonance spectrometry (MRS). The AT in the chow-fed Tg-$^{AT\text{-}hA2;}$ mA2$^{+/+}$ mice was 16% of the total body weight, and in the dox-fed Tg-$^{AT\text{-}hA2;}$ mA2$^{+/+}$ mice it increased by 2.5-fold–37.5% of the total body weight (Figures 1C and 1D).

The MRI/MRS observation was followed by AT histology and nuclear magnetic resonance (NMR) analysis to measure the total body lean mass, fat mass, and fluid in chow- and dox-fed Tg-$^{AT\text{-}hA2;}$ mA2$^{+/+}$ mice at 12 weeks (Figures 1E–1L). Panels E and I in Figure 1 show the body weight in both sexes. The Tg-$^{AT\text{-}hA2;}$ mA2$^{+/+}$ mice on the dox diet had significantly higher body weight when compared to chow-fed Tg-$^{AT\text{-}hA2;}$ mA2$^{+/+}$ mice, with the percent increase in body weight being the same in both sexes. There was also a significant increase in the lean mass of both male and female dox-fed Tg-$^{AT\text{-}hA2;}$ mA2$^{+/+}$ mice compared to chow-fed Tg-$^{AT\text{-}hA2;}$ mA2$^{+/+}$ mice (Figures 1F and 1J). The fat mass was significantly increased in dox-fed Tg-$^{AT\text{-}hA2;}$ mA2$^{+/+}$ mice compared to chow-fed Tg-$^{AT\text{-}hA2;}$ mA2$^{+/+}$ mice of both sexes (Figures 1G and 1K). Shown also is the relative distribution of lean, fat, and fluid mass expressed as the percent of total body weight (Figures 1H and 1L). About 12–15% of the total body weight is composed of bone, fur, claws, and so forth (marked as "other"). Figures 1M and 1N show histological images of the white and brown AT from chow- and dox-fed Tg-$^{AT\text{-}hA2;}$mA2$^{+/+}$ mice of both sexes at 12 weeks (Figure 1M), and only gonadal AT at 24 weeks (Figure 1N). We note that with the overexpression of h*AGPAT2* in both white and brown AT, the size of the adipocytes was enlarged in dox-fed compared to chow-fed Tg-$^{AT\text{-}hA2;}$mA2$^{+/+}$ mice (Figures S2A–S2H).

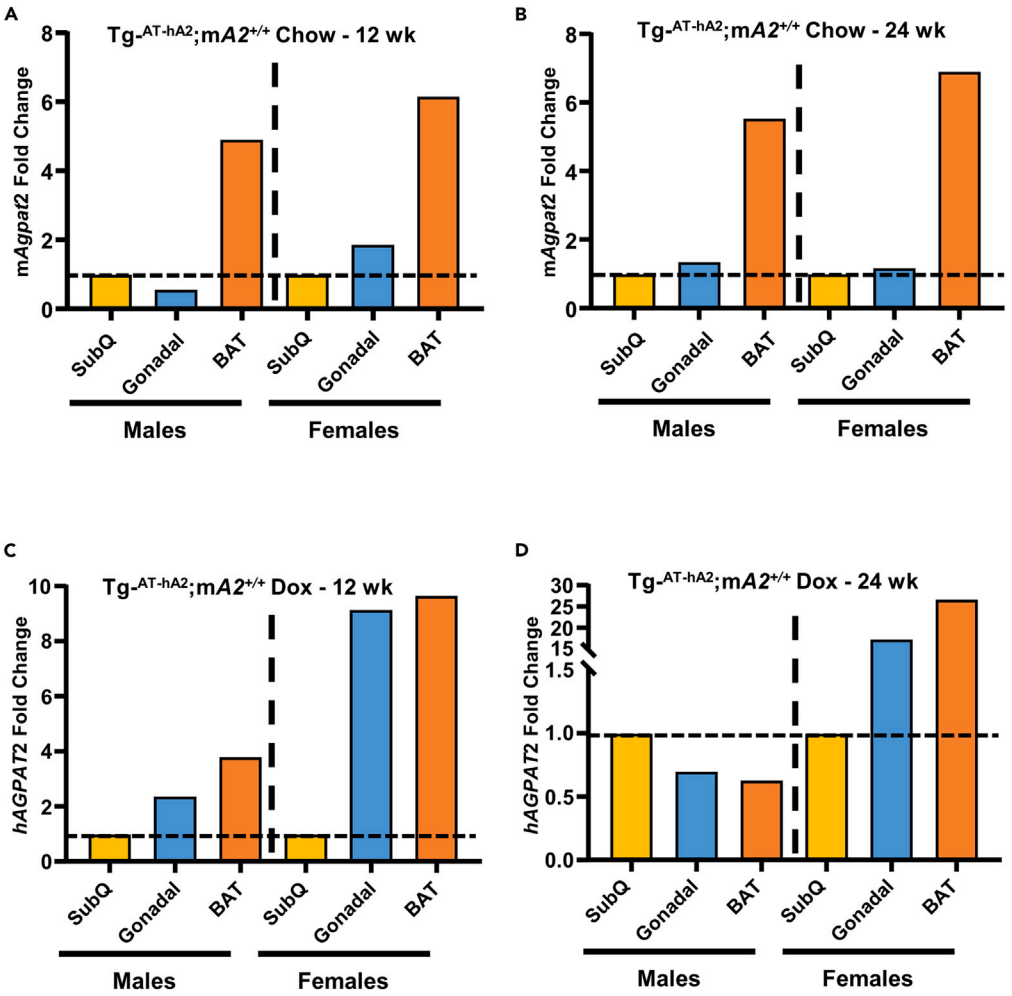

Figure 2. Expression of endogenous m*Agpat2* and the human transgene *AGPAT2* in adipose tissue depots in 12 and 24 weeks Tg-$^{AT\text{-}hA2}$;m*A2*$^{+/+}$ mice of both sexes

(A and B) The expression of endogenous m*Agpat2* is relative to the expression in subcutaneous (SubQ) adipose tissue = 1 for each sex. This clearly shows that the expression of m*Agpat2* in brown adipose tissue (BAT) is several fold more expressed than in SubQ or gonadal adipose tissue at both 12 and 24 weeks. The expression of m*Agpat2* is similar between the white adipose tissue depots (SubQ and gonadal) in both sexes.

(C and D) h*AGPAT2* expression follows a similar expression pattern to m*Agpat2*, except in male BAT at both 12 and 24 weeks. This data is extracted from Table S1 to emphasize the expression pattern of m*Agpat2* and h*AGPAT2* among the three adipose tissue depots studied. Tg-$^{AT\text{-}hA2}$;m*A2*$^{+/+}$ abbreviated to Tg-m*A2*$^{+/+}$.

Expression of mouse and human Agpat2 transcript in adipose tissue depots

Next, we quantified the transcripts for m*Agpat2* and h*AGPAT2* in the AT depots in chow- and dox-fed Tg-$^{AT\text{-}hA2}$;mA2$^{+/+}$ mice, respectively, at 12 and 24 weeks for both sexes (Figures 2A–2D). The expression of m*Agpat2* in brown adipose tissue (BAT) was several fold more expressed than in subcutaneous adipose tissue (SubQ) or gonadal adipose tissue at both 12 and 24 weeks in both sexes (Panel A-B). The expression of m*Agpat2* was similar between the white adipose tissue depots (SubQ and gonadal) in both sexes. Human *AGPAT2* expression followed a similar expression pattern to m*Agpat2*, except in females at 12 weeks, where the expression was highest in gonadal AT instead of BAT, and in males at 24 weeks, where expression was lowest in BAT (Panel C-D). It is to be noted that its own endogenous promoter drives the expression of m*Agpat2*, while the adiponectin/Tet-O/CMV promoters drive the expression of h*AGPAT2*.

B6/129 mice on doxycycline-containing diet only show a modest increase in body weight and adipose tissue but not glucose intolerance

These observations prompted us to ascertain whether the weight gain in these mice was due to the overexpression of h*AGPAT2* or due to the doxycycline antibiotic in the diet.[6] A previous investigation in humans administered the doxycycline antibiotic does report an increase in body weight, mostly attributing this to a change in the gut microbiota.[7] In another study, prescribing antibiotics to children early in life resulted in

weight gain.[8] Since our mice are housed in pathogen-free conditions and are fed a similar diet (chow vs. doxycycline, sterilized by irradiation), we do not expect any significant change in the gut microbiota.

We fed the same dox diet to naive B6/129 mice. The genetic background of B6/129 mice is closest to the background of the transgenic mice used in the current study. We started the dox diet at 2 weeks of age and initiated body weight measurement starting at 4 weeks of age and each week until 16 weeks of age. We did observe a slight increase in body weight of both the sexes in the dox-fed mice compared to the chow-fed mice at 12 weeks (Figures S3A and S3B), and this increase in body weight continued to increase until 24 weeks (Figures S3G and S3H).

The oral glucose tolerance test (OGTT) showed that the dox-fed B6/129 mice remained glucose sensitive at both 12 (Figures S3C and S3D) and 24 (Figures S3I and S3J) weeks in both the sexes. This suggests that while the continuous feeding of a dox-containing diet until 24 weeks did result in some body weight gain, it did not result in glucose intolerance at either 12 (Figures S3E and S3F) or 24 (Figures S3K–S3L) weeks. Therefore, the changes we note in the Tg-$^{AT\text{-}hA2;}$mA2$^{+/+}$ mice are due to the increase in expression of h*AGPAT2*, and not due to the doxycycline antibiotic-containing diet.

Measurement of key adipose tissue markers, *de novo* lipogenesis, fatty acid oxidation, lipolysis, and triacylglycerol synthesis transcripts in Tg-$^{AT\text{-}hA2}$;mA2$^{+/+}$ mice at 12 and 24 weeks

At 12 weeks, the key genes for adipocyte lineage, *de novo* lipogenesis, fatty acid oxidation, lipolysis, and TAG synthesis were measured in SubQ, gonadal, and BAT (Table 1). We observed that overexpression of h*AGPAT2* transcripts in dox-fed Tg-$^{AT\text{-}hA2;}$mA2$^{+/+}$ mice increased from 100 to 650-fold compared to chow-fed Tg-$^{AT\text{-}hA2;}$mA2$^{+/+}$ mice. We also observed expression of the transgene in chow-fed Tg-$^{AT\text{-}hA2;}$mA2$^{+/+}$ mice, although at a much lower level than dox-fed Tg-$^{AT\text{-}hA2;}$mA2$^{+/+}$ mice. This is most likely due to the leakiness of the expression construct being activated by the adiponectin promoter in these adipose depots.

Despite the increase in AT mass in dox-fed mice as measured by MRI, NMR, and observed visually, we did not note any increase in markers for adipocyte lineage, *de novo* lipogenesis, and TAG synthesis. In fact, the key genes in these pathways decreased, many of them decreased by more than 2-fold (Table 1). A possible explanation can be that by overexpressing h*AGPAT2* in AT, it redistributes the products of this enzyme, phosphatidic acid (PA), to additional pathways not determined in this study. Also not determined is whether re-expression of h*AGPAT2* from E13.5 resets the embryonic tissue imprinting, the consequence of which is a decrease in the expression of genes involved in the key pathways noted above.

Shown in Table S1 is the mRNA expression of similar genes at 24 weeks. Again, the overexpression of h*AGPAT2* transcripts in dox-fed Tg-$^{AT\text{-}hA2;}$ mA2$^{+/+}$ mice compared to chow-fed Tg-$^{AT\text{-}hA2;}$ mA2$^{+/+}$ mice was similar to the comparison at 12 weeks.

In the AT at both 12 and 24 weeks, *Mogat1* was not upregulated as seen in the fatty livers of *Agpat2*$^{-/-}$ mice,[3] while *Mogat2* was upregulated in the white AT depots (SubQ and gonadal), but not in BAT. This was more prominent in male mice than in female mice. However, female gonadal tissue was the only tissue where *Mogat2* was expressed in the chow-fed Tg-$^{AT\text{-}hA2;}$ mA2$^{+/+}$ mice, so the fold changes are only approximations. Therefore, we can only say that the genes are upregulated in the dox-fed Tg-$^{AT\text{-}hA2;}$mA2$^{+/+}$ mice.

Increased mRNA expression of markers for inflammation in the adipose tissue of dox-fed Tg-$^{AT\text{-}hA2}$;mA2$^{+/+}$ mice at 12 and 24 weeks of both sexes

Normally, the expansion of AT (either by hyperplasia or hypertrophy), as in obesity, attracts macrophage infiltration,[9] although this is more common in obese AT than in lean AT. This prompted us to measure a few of the inflammatory markers in the AT in all three depots of both sexes at 12 and 24 weeks (Table 2). These inflammation markers, *Il-6*, *Tnfα*, *Ccl2*, and *Ccl4*, were selected based on previous reports in obese AT.[10]

At 12 and 24 weeks in both sexes, *Il-6* was not expressed in any AT depot (C_t>30). Like *Il-6*, *Ccl4* was also not expressed in females at 12 and 24 weeks in all depots. For males, it was barely expressed (C_t ~29) in the dox-fed Tg-$^{AT\text{-}hA2}$;mA2$^{+/+}$ mice for SubQ at 12 weeks, and all 3 AT depots at 24 weeks. A caution that the fold increase in the dox-fed Tg-$^{AT\text{-}hA2}$;mA2$^{+/+}$ mice might not reflect the real increase due to the low expression of these markers in chow-fed Tg-$^{AT\text{-}hA2}$;mA2$^{+/+}$ mice of either sex. *Ccl2*, another chemokine, was detected in most AT examined here except BAT of chow-fed Tg-$^{AT\text{-}hA2}$;mA2$^{+/+}$ mice at 12 weeks for both sexes, SubQ of chow-fed Tg-$^{AT\text{-}hA2}$;mA2$^{+/+}$ female mice at 24 weeks, and BAT of chow-fed Tg-$^{AT\text{-}hA2}$;mA2$^{+/+}$ mice of both sexes. *Ccl2* expression increased by ~ 1- to 4-fold in SubQ, ~2– to 8-fold in gonadal tissue, and markedly in BAT (5– to 13-fold) of dox-fed Tg-$^{AT\text{-}hA2}$;mA2$^{+/+}$ mice. This pattern was also observed with the expression of *Tnfα*. The presence of these inflammatory markers in newly generated AT depots of dox-fed Tg-$^{AT\text{-}hA2}$;mA2$^{+/+}$ mice would indicate potentially dysfunctional adipose tissue. Inflammation from dying cells can attract adipose tissue macrophages (ATMs) in order to remove the dead adipocytes. Nevertheless, a prior report indicates the beneficial role of these monocytes/macrophages critical in the development/maintenance of AT.[11] In another study where human adipose-derived stem cells and human umbilical vein endothelial cells were co-cultured, *Ccl2* was essential for adipogenesis and angiogenesis.[12]

Why is there an increase in adipose tissue mass and adipose cell size in dox-fed Tg-$^{AT\text{-}hA2}$;mA2$^{+/+}$ mice?

To investigate this further, we studied AT hyperplasia and cell size in all three AT depots. An increase in AT mass can result via two routes: a) an increase in cell mass (hyperplasia) or b) an increased synthesis of cellular TAG. As shown later (see Figures 3B and 3C), an increase in TAG synthesis is not the case. We then addressed whether increased hyperplasia is the cause by measuring the expression of key DNA polymerases, which will reflect increased DNA synthesis as a surrogate reporter for hyperplasia. There are a large number of DNA polymerases

Table 1. RT-qPCR measurements of key genes for pathways of adipocyte lineage, *de novo* lipogenesis, triacylglycerol synthesis, fatty acid oxidation, and lipolysis in AT of 12 weeks chow- and doxycycline-fed Tg-$^{AT\text{-}hA2}$;m$A2^{+/+}$ mice

Tissue	SubQ				Gonadal				BAT			
Sex	Male		Female		Male		Female		Male		Female	
Genotype	Tg-m$A2^{+/+}$		Tg-m$A2^{+/+}$		Tg-m$A2^{+/+}$		Tg-m$A2^{+/+}$		Tg-m$A2^{+/+}$		Tg-m$A2^{+/+}$	
Diet	Chow	Dox	Chow	Dox	Chow	Dox	Chow	Dox	Chow	Dox	Chow	Dox
samples pooled (n)	4	4	4	4	3	4	4	4	4	4	4	4
Gene/fold change												
Adipocyte lineage												
Ap2	1.00	0.25	1.00	0.34	1.00	0.72	1.00	0.52	1.00	0.77	1.00	0.75
Cebpα	1.00	0.19	1.00	0.38	1.00	0.46	1.00	0.32	1.00	0.52	1.00	0.78
Pparγ	1.00	0.28	1.00	0.41	1.00	0.51	1.00	0.43	1.00	0.64	1.00	0.72
Perilipin 1	1.00	0.24	1.00	0.41	1.00	0.46	1.00	0.41	1.00	0.68	1.00	0.95
Pref 1	1.00	**0.38**	**1.00**	**1.15**	1.00	0.33	1.00	0.54	1.00	1.18	1.00	**0.76**
De Novo Lipogenesis												
Acc1	1.00	0.07	1.00	0.06	1.00	0.43	1.00	0.08	1.00	0.50	1.00	0.75
Acc2	1.00	0.05	1.00	0.03	1.00	0.36	1.00	0.09	1.00	0.45	1.00	0.71
Acly	1.00	0.08	1.00	0.08	1.00	0.67	1.00	0.07	1.00	0.45	1.00	0.67
Elovl6	1.00	0.05	1.00	0.05	1.00	0.74	1.00	0.05	1.00	0.50	1.00	0.74
Fas	1.00	0.08	1.00	0.08	1.00	0.60	1.00	0.10	1.00	0.38	1.00	0.72
Scd 1	1.00	0.13	1.00	0.17	1.00	0.46	1.00	0.19	1.00	0.65	1.00	1.19
Scd 2	1.00	0.40	1.00	0.41	1.00	2.01	1.00	0.43	1.00	0.80	1.00	0.86
Triacylglycerol Synthesis												
hAGPAT2	1.00	159.87	1.00	107.19	1.00	492.44	1.00	127.87	1.00	561.11	1.00	646.49
mAgpat2	1.00	0.22	1.00	0.11	1.00	0.85	1.00	0.25	1.00	0.65	1.00	0.58
Mogat1	1.00	0.23	1.00	0.14	1.00	0.70	1.00	0.41	1.00	0.15	1.00	**0.16**
Mogat2	1.00	2.71	1.00	0.70	**1.00**	4.53	1.00	1.55	1.00	0.81	1.00	0.21
Dgat1	1.00	0.29	1.00	0.34	1.00	0.63	1.00	0.51	1.00	0.60	1.00	0.61
Dgat2	1.00	0.41	1.00	0.27	1.00	1.51	1.00	0.42	1.00	0.62	1.00	0.41
Fatty Acid Oxidation												
Pparα	1.00	0.05	1.00	0.06	1.00	0.42	1.00	0.21	1.00	0.66	1.00	1.24
Cpt1a	1.00	1.01	1.00	1.18	1.00	0.93	1.00	1.60	1.00	1.85	1.00	2.54
Cpt1b	1.00	0.13	1.00	0.10	1.00	1.70	1.00	0.27	1.00	0.75	1.00	0.82
Cpt2	1.00	0.27	1.00	0.34	1.00	0.71	1.00	0.45	1.00	0.84	1.00	1.00
Acox1	1.00	0.31	1.00	0.44	1.00	0.86	1.00	0.63	1.00	0.78	1.00	0.92
Mcad	1.00	0.22	1.00	0.34	1.00	0.65	1.00	0.51	1.00	0.68	1.00	0.71
Vlcad	1.00	0.37	1.00	**0.30**	1.00	1.17	1.00	0.41	1.00	1.05	1.00	0.82
Lipolysis												
Atgl	1.00	0.18	1.00	0.35	1.00	0.58	1.00	0.42	1.00	0.67	1.00	0.91
Hsl	1.00	0.21	1.00	0.32	1.00	0.40	1.00	0.42	1.00	0.65	1.00	0.84
Mgll	1.00	0.33	1.00	0.45	1.00	0.64	1.00	0.55	1.00	0.86	1.00	1.32

An equal quantity of total RNA was pooled from each mouse (n = 3–4) and quantified once in duplicate. Data are shown compared to chow-fed Tg-$^{AT\text{-}hA2}$;m$A2^{+/+}$ mice = 1. Bold text indicates a raw C_t value >30. Wherever the raw C_t value >30, we consider the fold change as approximate. For the human transgene *hAGPAT2*, the raw C_t values are as follows: in male SubQ, chow-fed C_t = 26.03, dox-fed C_t = 18.32; in gonadal tissue, chow-fed C_t = 25.28, dox-fed C_t = 16.15; in BAT, chow-fed C_t = 26.44, dox-fed C_t = 17.23. C_t values were similar for the females. SubQ, subcutaneous adipose tissue; gonadal, gonadal adipose tissue; BAT, brown adipose tissue. Tg-$^{AT\text{-}hA2}$;m$A2^{+/+}$ abbreviated to Tg-m$A2^{+/+}$.

Table 2. RT-qPCR measurements of select genes for inflammation in adipose tissue depots of 12 and 24 weeks chow- and doxycycline (dox)-fed Tg-$^{AT\text{-}hA2}$;$mA2^{+/+}$ mice

Duration	12 weeks				24 weeks			
Genotype	Tg-$mA2^{+/+}$							
Sex	Male		Female		Male		Female	
Diet	Chow	Dox	Chow	Dox	Chow	Dox	Chow	Dox
Tissue	**SubQ**							
Samples pooled (n)	4	4	4	4	3	4	5	6
Il-6	**1.00**	**0.55**	**1.00**	**2.02**	**1.00**	**2.14**	**1.00**	**0.33**
Tnfα	1.00	5.17	1.00	1.49	**1.00**	1.25	1.00	2.19
Ccl2	1.00	1.11	1.00	1.39	1.00	4.01	1.00	**1.54**
Ccl4	**1.00**	1.81	**1.00**	**0.95**	**1.00**	1.69	**1.00**	**1.23**
Tissue	**Gonadal**							
Samples pooled (n)	3	4	4	4	3	4	5	6
Il-6	**1.00**	**1.18**	**1.00**	**2.72**	**1.00**	**4.13**	**1.00**	**3.53**
Tnfα	**1.00**	4.70	**1.00**	1.76	**1.00**	12.15	**1.00**	**7.33**
Ccl2	1.00	2.02	1.00	2.69	1.00	8.68	1.00	3.52
Ccl4	**1.00**	**1.63**	**1.00**	**1.98**	**1.00**	10.01	**1.00**	**7.56**
Tissue	**BAT**							
Samples pooled (n)	4	4	4	4	3	4	5	6
Il-6	**1.00**	**10.78**	**1.00**	**2.95**	**1.00**	**1.43**	**1.00**	**3.90**
Tnfα	**1.00**	25.29	**1.00**	6.65	**1.00**	29.44	**1.00**	**6.89**
Ccl2	**1.00**	11.16	**1.00**	5.36	**1.00**	13.23	**1.00**	**2.57**
Ccl4	**1.00**	**7.29**	**1.00**	**9.08**	**1.00**	19.02	**1.00**	**5.29**

An equal quantity of total RNA was pooled from each mouse (n = 3–4) and quantified once in duplicate. Data are shown compared to chow-fed WT mice = 1. Bold text indicates a raw C_t value >30. Wherever the raw C_t value >30, we consider the fold change as approximate. SubQ, subcutaneous adipose tissue; gonadal, gonadal adipose tissue; BAT, brown adipose tissue. **WT - Tg-$^{AT\text{-}hA2}$;$mA^{+/+}$** is abbreviated to **Tg-$mA2^{+/+}$**.

involved in eukaryotic DNA replication;[13–16] critical among these is *Polα*, composed of multiple subunits that initiates DNA priming (primase) and *Pole*, also composed of several subunits, in DNA replication. These two polymerases account for ~90% of DNA synthesis.[15] As shown in Table 3, one of the key polymerases, *Polα*, was increased at 12 weeks and more so at 24 weeks in all three depots and in both sexes, which suggests an increase in cell number.

We also noted an increase in adipocyte cell size (Figure S2), which in the past has been associated with dysfunctional adipocytes. We believe this can also be a simple case of cell size increase independent of TAG synthesis and adipocyte dysfunction. A previous report also indicates that newly generated adipocytes are of larger size.[17] Although there is an increase in AT per se, there is no correlation between the increase in AT and an increase in cell size. For example, in hepatic steatosis, hepatocytes are filled with lipid droplets (containing TAG), but no increase in cell size is noted. Therefore, the increase in cell size can be independent of TAG accumulation in AT. We carried out a literature search on the molecular mechanism of cell size increase and were surprised that there is very little consensus on this issue. A recent report on cell size and growth did not reach a consensus regarding the tissue growth versus cell size.[18,19] Thus, gene markers for cell size alone are not well defined. There is mention of a gene *Whi5*,[20] a transcriptional regulator in yeast that regulates cell size; the mouse homolog[21] of the gene is *Rb1* (retinoblastoma-associated protein 1) which remains unremarkable in our study (Table 3).

Protein measurements in male adipose tissue at 12 weeks by tandem mass tag-mass spectrometry (TMT-MS)

To complement the mRNA expression, we measured protein expression in 12 weeks old male AT lysates from dox-fed ***Tg-$^{AT\text{-}hA2}$;$mA2^{+/+}$*** mice and compared them to those from 12 weeks chow-fed ***Tg-$^{AT\text{-}hA2}$;$mA2^{+/+}$*** mice employing TMT-MS.[22,23] We employed this method chiefly to a) measure multiple proteins from limited tissue samples, and b) identify protein-specific peptides, eliminating the need to use highly characterized antibodies, which are not available for all proteins. As shown in Table 4, human AGPAT2 transgene expression was increased several fold (10– to 19-fold) in dox-fed compared to chow-fed ***Tg-$^{AT\text{-}hA2}$;$mA2^{+/+}$*** mice in all 3 AT depots, which is consistent with the increased expression of mRNA (Table 1). We also noted differential protein expression among the 3 adipose depots. Elovl6 was not detected in WAT but was detected in BAT. Mogat1 was not detected in gonadal AT or BAT, but was detected in SubQ AT. Cpt1b, Ucp1, and Ucp3 were

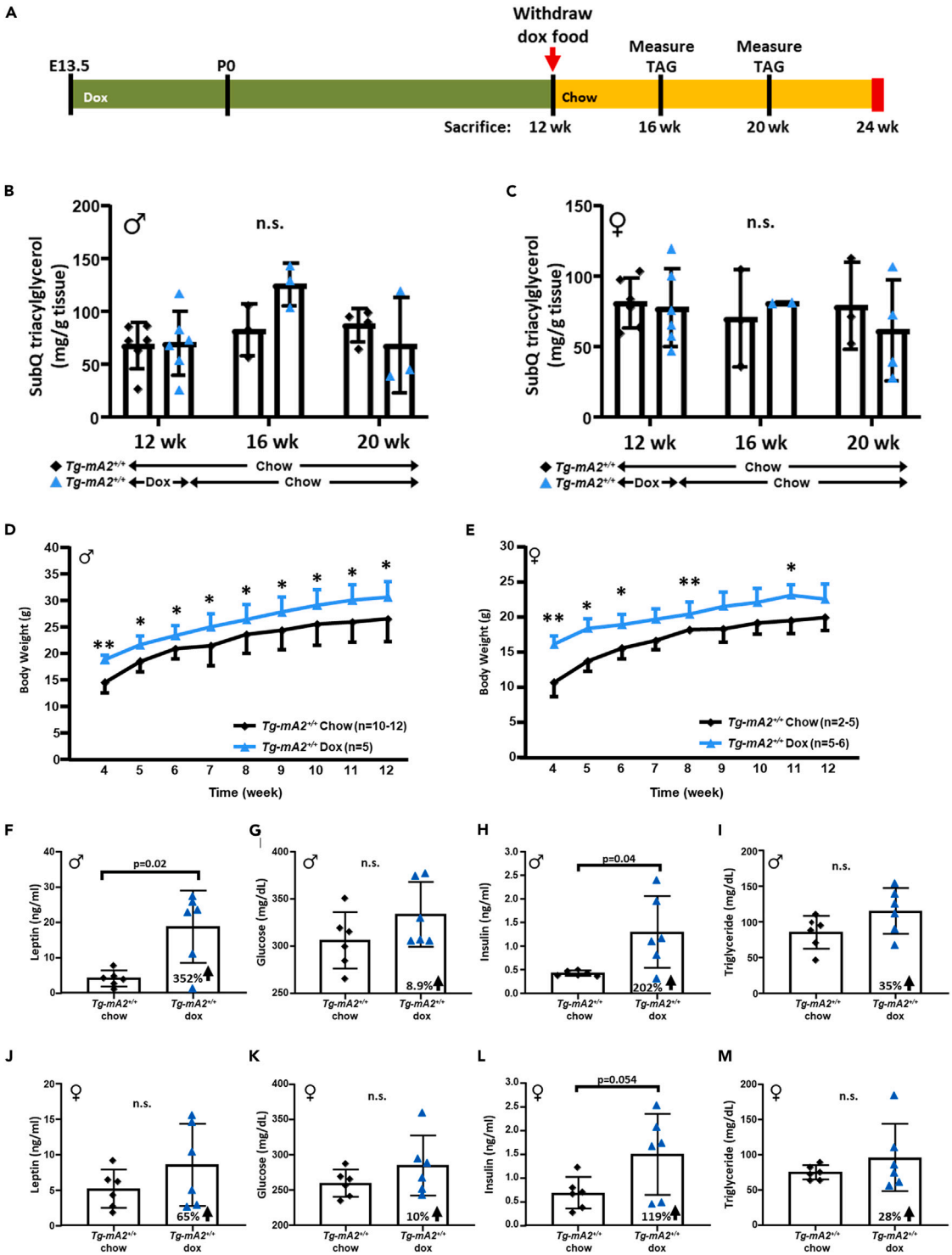

Figure 3. Triacylglycerol levels in subcutaneous adipose tissue (SubQ) of doxycycline-fed (dox) Tg-$^{AT\text{-}hA2}$;$mA2^{+/+}$ mice did not change compared to non-overexpressing Tg-$^{AT\text{-}hA2}$;$mA2^{+/+}$ in 12 week old mice

(A) The strategy for dox-fed Tg-$^{AT\text{-}hA2}$;$mA2^{+/+}$ mice with subsequent removal (to turn off hAGPAT2 expression in AT).

(B and C) Quantitation of total triacylglycerol (TAG) in SubQ AT at 12 weeks of dox feeding, 16 weeks (4 weeks post-dox removal), and 20 weeks (8 weeks post-dox removal). Even after 12 weeks of overexpression, there was no significant difference between the SubQ TAG levels in chow-fed and dox-fed Tg-$^{AT\text{-}hA2}$;$mA2^{+/+}$ mice. Consequently, there is also no difference between the 2 groups after removal of the dox food (turning off hAGPAT2 expression) at both 16 weeks and

Figure 3. *Continued*

20 weeks. In chow-fed Tg-$^{AT\text{-}hA2}$;*mA2*$^{+/+}$ mice, AGPAT2 does not appear to contribute toward TAG synthesis. The data are represented as mean ± SD. P-values were determined using two-way ANOVA.

(D and E) The body weight for groups of (D) male and (E) female Tg-$^{AT\text{-}hA2}$;*mA2*$^{+/+}$ mice of both sexes were measured weekly at 4 weeks through 12 weeks. Doxycycline-fed (dox) Tg-$^{AT\text{-}hA2}$;*mA2*$^{+/+}$ mice show increased body weight compared to chow-fed Tg-$^{AT\text{-}hA2}$;*mA2*$^{+/+}$ mice. The data are represented as mean ± SD. P-values were determined using mixed model repeated measurements to compare the trend of body weight changes over time between treatment groups. *$p < 0.05$, **$p < 0.001$, ***$p < 0.0001$.

(F and J) An increase in leptin levels were observed in (F) male and (J) female dox-fed Tg-$^{AT\text{-}hA2}$;*mA2*$^{+/+}$ mice compared to chow-fed Tg-$^{AT\text{-}hA2}$;*mA2*$^{+/+}$ mice of both sexes, but this was only significant for males.

(G and K) A mild but statistically insignificant increase in non-fasting glucose levels was noted in both (G) males and (K) females.

(H and L) Dox-fed Tg-$^{AT\text{-}hA2}$;*mA2*$^{+/+}$ (H) male and (L) female mice also show increased insulin levels compared to chow-fed Tg-$^{AT\text{-}hA2}$;*mA2*$^{+/+}$ mice, but reached statistical significance only in male mice.

(I and M) There is no significant change in plasma triglycerides of (I) males or (M) females. The data are represented as mean ± SD. Each symbol represents individual measurements. Percent increase between chow-fed and dox-fed Tg-$^{AT\text{-}hA2}$;*mA2*$^{+/+}$ mice are shown in the bars. P-values were determined using the Student's *t* test. Individual values are shown. n = 2–6. n.s., not significant. Tg-$^{AT\text{-}hA2}$;*mA2*$^{+/+}$ abbreviated to Tg-m*A2*$^{+/+}$. See also Figure S5.

undetectable only in gonadal AT, but detected in SubQ AT and BAT. The detection of polymerases was mixed. In BAT, none of the polymerases were detected, while in WAT (SubQ and gonadal), some subunits of polymerases were detected. Proteins of oxidative phosphorylation (OXPHOS) were detectable in all the AT depots, but did not change in dox-fed compared to chow-fed *Tg-*$^{AT\text{-}hA2}$*;mA2*$^{+/+}$ mice. A few proteins could not be detected by this method, although they were present in mRNA.

Analysis of phospholipids and neutral lipids in adipose tissue depots in male chow- and doxycycline-fed Tg-$^{AT\text{-}hA2}$;mA2$^{+/+}$ mice at 12 weeks

The product of the AGPAT2 enzyme (phosphatidic acid) is an important phospholipid involved in signaling, the generation of various phospholipids such as phosphatidylcholine (PC), phosphatidylethanolamine (PE), phosphatidylinositol (PI) and likely the synthesis of TAG. Therefore, overexpressing this enzyme in AT should reveal differences in phospholipid levels and its molecular species. We analyzed this by lipid mass spectrometry, as shown in Figure S4. We did not note any significant changes in any of the major phospholipid classes between chow- and dox-fed *Tg-*$^{AT\text{-}hA2}$*;mA2*$^{+/+}$ except for PE and PI in BAT, where they were decreased in dox-fed *Tg-*$^{AT\text{-}hA2}$*;mA2*$^{+/+}$ compared to chow-fed mice (Figure S4). Still more surprising was the data for neutral lipids. If the notion that this enzyme is a TAG synthesis enzyme is true, we would expect that by overexpressing h*AGPAT2* in AT would result in an increase in DAG and TAG. However, in our analysis, this was not the case (Figure S4). Next, we measured the mRNA expression of key lipases for TAG degradation[24] in all three AT depots at 12 weeks (Table 1) and 24 weeks (Table S1) and noted no increase in their expression. This suggests that TAG modulation is not due to lipolysis. There was a decrease in ceramides noted for dox-fed *Tg-*$^{AT\text{-}hA2}$*;mA2*$^{+/+}$mice, but again only for BAT. From this analysis, we could summarize that most likely, the role of AGPAT2 in synthesizing TAG is minimal at best and is more for generating phospholipids and adipogenesis.

Triacylglycerol levels in subcutaneous adipose tissue of doxycycline-fed (dox) Tg-$^{AT\text{-}hA2}$;mA2$^{+/+}$ mice did not change compared to chow-fed Tg-$^{AT\text{-}hA2}$;mA2$^{+/+}$ mice or upon turning off the expression of h*AGPAT2*

We measured the TAG concentration in SubQ tissue, a fat depot known to synthesize TAG. In this experiment, we initially turned on the expression of h*AGPAT2* (with the dox diet) for 12 weeks followed by turning off the expression of h*AGPAT2* by withdrawing the dox diet and providing the chow diet and measuring the TAG after 4 weeks and 8 weeks (see schematics for food withdrawal (Figure 3A)). In this experimental set up and measuring the TAG concentration by a biochemical method, we observed no significant changes in TAG levels between chow-fed and dox-fed mice, either after 12 weeks of turning on the h*AGPAT2* expression or upon turning off the h*AGPAT2* expression (Figures 3B and 3C). This observation further indicates the role of *AGPAT2* more for phospholipid synthesis and minimal, at best, for TAG synthesis.

Increased adiposity in dox-fed Tg-$^{AT\text{-}hA2}$;mA2$^{+/+}$ mice show sex-specific alterations in body weight, leptin, and insulin levels at 12 and 24 weeks

Next, we measured a few parameters in dox-fed *Tg-*$^{AT\text{-}hA2}$*;mA2*$^{+/+}$ mice compared to chow-fed *Tg-*$^{AT\text{-}hA2}$*;mA2*$^{+/+}$ mice. Chow- and dox-fed Tg-$^{AT\text{-}hA2}$;*mA2*$^{+/+}$ mice were weighed weekly starting at 4 weeks (once the genotyping was completed) until 12 weeks for both sexes (Figures 3D and 3E). The Tg-$^{AT\text{-}hA2}$;*mA2*$^{+/+}$ mice of both sexes gained body weight when kept on dox food (which allows re-expression of h*AGPAT2* in AT). We then measured the non-fasting plasma leptin (Figures 3F and 3J). Compared to chow-fed Tg-$^{AT\text{-}hA2}$;*mA2*$^{+/+}$ mice, there was an increase in plasma leptin levels in dox-fed Tg-$^{AT\text{-}hA2}$;*mA2*$^{+/+}$ mice (M:352% increase, F:65% increase); although it only reached statistical significance in the males due to wide individual variation in the female mice. The plasma glucose levels were mildly elevated in dox-fed Tg-$^{AT\text{-}hA2}$;*mA2*$^{+/+}$ mice, but remained statistically insignificant (Figures 3G and 3K). Unexpectedly, based on plasma glucose levels, we were not expecting insulin levels to increase. However, the insulin levels did rise significantly in both sexes of dox-fed Tg-$^{AT\text{-}hA2}$;*mA2*$^{+/+}$ mice (Figures 3H and 3L). The plasma triglyceride levels did not change (Figures 3I and 3M). Again, 12 weeks of dox-feeding did not result in any changes in the non-fasting plasma glucose or TAG.

Table 3. RT-qPCR measurements of select genes for hyperplasia (polymerases) in adipose tissue depots of 12 and 24 weeks chow-fed WT and doxycycline (dox)-fed Tg-$^{AT\text{-}hA2}$;m$A2^{+/+}$ mice

Duration	12 weeks				24 weeks			
Genotype	Tg-m$A2^{+/+}$							
Sex	Male		Female		Male		Female	
Diet	Chow	Dox	Chow	Dox	Chow	Dox	Chow	Dox
Tissue	SubQ							
Samples pooled (n)	4	4	4	4	3	4	5	6
Pola1	**1.00**	**0.94**	**1.00**	**0.63**	**1.00**	**6.37**	**1.00**	**5.91**
Pola2 323	1.00	1.42	1.00	0.77	1.00	0.40	1.00	**1.14**
Pola2 431	1.00	1.23	1.00	1.64	1.00	0.60	1.00	**4.35**
Prim1	1.00	1.19	1.00	1.94	1.00	0.34	1.00	1.12
Prim2	1.00	1.29	1.00	0.78	1.00	1.07	1.00	1.18
Pole	**1.00**	**1.83**	**1.00**	**0.71**	**1.00**	**0.16**	**1.00**	**2.10**
Pole2	1.00	1.84	1.00	**0.86**	1.00	0.76	1.00	**1.56**
Pole3	1.00	0.91	**1.00**	**1.29**	**1.00**	**0.33**	**1.00**	**0.84**
Pole4	1.00	1.06	1.00	0.86	**1.00**	**0.52**	**1.00**	**0.67**
Rb1	1.00	0.79	1.00	0.52	1.00	0.91	1.00	0.89
Tissue	Gonadal							
Samples pooled (n)	3	4	4	4	3	4	5	6
Pola1	**1.00**	**0.70**	**1.00**	**2.14**	**1.00**	**0.64**	**1.00**	**3.27**
Pola2 323	1.00	0.94	1.00	0.90	1.00	1.15	1.00	1.09
Pola2 431	1.00	0.88	1.00	0.93	1.00	0.96	1.00	0.91
Prim1	1.00	1.08	1.00	1.20	1.00	1.35	1.00	1.77
Prim2	1.00	1.04	1.00	1.21	1.00	1.07	1.00	1.81
Pole	**1.00**	**0.91**	**1.00**	**0.87**	**1.00**	**0.74**	**1.00**	**3.53**
Pole2	1.00	1.31	1.00	**2.26**	**1.00**	2.03	1.00	2.11
Pole3	1.00	0.52	1.00	**0.80**	**1.00**	**0.43**	**1.00**	**1.47**
Pole4	1.00	0.32	1.00	0.54	**1.00**	**0.39**	1.00	**1.31**
Rb1	1.00	0.63	1.00	0.70	1.00	0.56	1.00	0.75
Tissue	BAT							
Samples pooled (n)	4	4	4	4	3	4	5	6
Pola1	**1.00**	**0.72**	**1.00**	**2.13**	**1.00**	**1.57**	**1.00**	**2.29**
Pola2 323	1.00	1.30	1.00	2.35	**1.00**	1.19	**1.00**	**0.82**
Pola2 431	1.00	0.92	1.00	1.23	**1.00**	**1.23**	**1.00**	**0.33**
Prim1	1.00	1.09	1.00	0.95	1.00	0.96	1.00	**1.00**
Prim2	1.00	1.42	1.00	1.81	1.00	1.56	1.00	**1.26**
Pole	**1.00**	**1.74**	**1.00**	**3.83**	**1.00**	**25.74**	**1.00**	**3.15**
Pole2	1.00	1.92	1.00	2.23	**1.00**	**1.90**	**1.00**	**1.49**
Pole3	1.00	**0.46**	1.00	**0.45**	**1.00**	**1.31**	**1.00**	**0.52**
Pole4	**1.00**	1.46	**1.00**	**0.89**	**1.00**	**0.95**	**1.00**	**0.89**
Rb1	1.00	0.75	1.00	1.59	1.00	0.71	1.00	0.52

An equal quantity of total RNA was pooled from each mouse (n = 3–6) and quantified once in duplicate. Data are shown compared to chow-fed WT mice = 1. Bold text indicates a raw C_t value >30. Wherever the raw C_t value >30, we consider the fold change as approximate. Note: we amplified *Pola2* using two primer pairs (*Pola2* 323 and *Pola2* 431). SubQ, subcutaneous adipose tissue; gonadal, gonadal adipose tissue; BAT, brown adipose tissue. **WT - Tg-$^{AT\text{-}hA2}$;m$A^{+/+}$** is abbreviated to **Tg-m$A2^{+/+}$**.

Table 4. Measurements of select proteins in adipose tissue depots of 12 weeks chow-fed and doxycycline (dox)-fed Tg-$^{AT\text{-}hA2}$;$mA2^{+/+}$ male mice by tandem mass tag (TMT) mass spectrometry (TMT-MS)

Tissue			SubQ				Gonadal				BAT			
Protein name	Protein Accession	Peptide sequence [AA-AA]	PSM	Unique peptide #	Chow (n=3)	Dox (n=3)	PSM	Unique peptide #	Chow (n=3)	Dox (n=3)	PSM	Unique peptide #	Chow (n=3)	Dox (n=3)
					Fold Change				Fold Change				Fold Change	
Adipocyte lineage														
Ap2	*P04117*	*SIITLDGGALVQVQK [83–97]*	*2071*	*14*	1.00	0.53‡	*2790*	*18*	1.00	1.27	*2216*	*17*	1.00	0.88
Cebpα	*P53566*	*TGGGGGGSGAGAGK [261–274]; VLELTSDNDR [315–324]*	*1*	*1*	1.00	0.36	*4*	*2*	1.00	1.14	*1*	*1*	1.00	0.99
Perilipin 1	*Q8CGN5*	*ETAEYAANTR [159–168]*	*172*	*31*	1.00	0.84	*171*	*29*	1.00	0.94	*329*	*33*	1.00	1.33
De Novo Lipogenesis														
Acc1	*Q5SWU9*	*IIQQAGQVWFPDSAFK [2009–2024]*	*251*	*69*	1.00	0.76	*236*	*66*	1.00	0.88	*1398*	*120*	1.00	0.72
Acc2	*E9Q4Z2*	*LLYGESPWGVTPIPFETPLSPPIAR [611–635]*	*68*	*8*	1.00	0.85	*63*	*11*	1.00	1.06	*593*	*85*	1.00	0.86
Acly	*Q91V92*	*GQELIYAGMPITEVFK [839–854]*	*514*	*67*	1.00	0.37	*573*	*67*	1.00	0.76	*3103*	*81*	1.00	0.57*
Elovl6	Q920L5	QFNENEAIQWMQENWK [16–31]	ND	ND	ND	ND	ND	ND	ND	ND	21.00	3.00	1.00	0.90
Fas	*P19096*	*LLLEVSYEAIVDGGINPASLR [81–101]*	*2174*	*142*	1.00	0.45	*2137*	*139*	1.00	1.08	*7817*	*160*	1.00	0.58*
Scd 1	*P13516*	*EDIHDPTYQDEEGPPPK [48–64]*	*19*	*3*	1.00	0.74	*15*	*3*	1.00	0.79	*67*	*6*	1.00	0.95
Scd 2	*P13011*	*TGDGSCK [350–356]*	*4*	*1*	1.00	0.76	*3*	*1*	1.00	0.84	*26*	*2*	1.00	0.77
Triacylglycerol Synthesis														
hAgpat2	*O15120*	*SSTAMTVMADLGER [146–159]*	*52*	*5*	1.00	17.00‡	*64*	*7*	1.00	9.85	*79*	*8*	1.00	19.08‡
mAgpat2	*Q8K3K7*	*VQVLDAVPTNGLTDADVTK [225–243]*	*41*	*8*	1.00	0.91*	*27*	*5*	1.00	1.03	*86*	*11*	1.00	1.09
mAgpat10	*Q8C0N2*	*YNPQFGDAFWNSSK [333–346]*	*22*	*9*	1.00	1.60	*20*	*8*	1.00	1.27	*11*	*5*	1.00	1.88*
Mogat1	*Q91ZV4*	*TPEQGGR [64–70]*	*1*	*1*	1.00	0.57	*ND*	*ND*	ND	ND	*ND*	*ND*	ND	ND
Dgat1	*Q9Z2A7*	*VSGAAAQQAVSYPDNLTYR [243–261]*	*30*	*10*	1.00	0.78	*19*	*10*	1.00	0.84	*40*	*13*	1.00	0.98
Dgat2	*Q9DCV3*	*QVIFEEGSWGR [287–297]*	*6*	*2*	1.00	1.15	*6*	*4*	1.00	0.96	*14*	*6*	1.00	1.79
Fatty Acid Oxidation														
Cpt1a	*P97742*	IPGEETDTIQHVK [317–329]	*29*	*13*	1.00	1.67	*29*	*13*	1.00	1.26	*21*	*7*	1.00	1.56
Cpt1b	*Q924X2*	*TSPDAFVQIALQLAHFR [564–580]*	*12*	*8*	1.00	1.97	*ND*	*ND*	ND	ND	*184*	*29*	1.00	1.61
Cpt2	*P52825*	*GVTLPELYQDPAYQR [567–581]*	*109*	*30*	1.00	0.73	*88*	*27*	1.00	1.16	*239*	*35*	1.00	1.20
Acox1	*Q9R0H0*	*EIENLILNDPDFQHEDYNFLTR [35–56]*	*189*	*37*	1.00	1.33*	*274*	*40*	1.00	3.27	*174*	*31*	1.00	1.90$
Mcad	*P45952*	*QEPGLGFSFELTEQQK [31–46]*	*158*	*26*	1.00	0.80	*212*	*29*	1.00	1.21	*661*	*35*	1.00	1.12
Vlcad	*P50544*	*EATQAVLDKPETLSSDASTR [44–63]*	*155*	*38*	1.00	0.99	*116*	*36*	1.00	1.20	*927*	*48*	1.00	1.23

(*Continued on next page*)

Table 4. *Continued*

Tissue			SubQ				Gonadal				BAT			
Protein name	Protein Accession	Peptide sequence [AA-AA]	PSM	Unique peptide #	Chow (n=3)	Dox (n=3)	PSM	Unique peptide #	Chow (n=3)	Dox (n=3)	PSM	Unique peptide #	Chow (n=3)	Dox (n=3)
					Fold Change				Fold Change				Fold Change	
Lipolysis														
Atgl	Q8BJ56	YVDGGISDNLPLYELK [164–179]	24	9	1.00	0.64	25	11	1.00	0.74	77	18	1.00	0.92
Hsl	P54310	VPDGIMAAYPVTTLQSSASPSR [443–464]	148	31	1.00	0.86	162	33	1.00	0.91	224	40	1.00	0.95
Mgll	O35678	DVLQHVDTIQK [115–125]	85	17	1.00	0.92	86	17	1.00	1.18	81	18	1.00	1.86
Polymerase														
Prim1	P20664	SGIVEYLSLVK [183–193]	1	1	1.00	1.46*	ND	ND	ND	ND	ND	ND	ND	ND
Prim2	P33610	GTEQYQSK [66–73]	4	3	1.00	1.88‡	2	2	1.00	0.91	ND	ND	ND	ND
Pole3	Q9JKP7	EALPDGVNISK [21–31]	ND	ND	ND	ND	2	1	1.00	1.01	ND	ND	ND	ND
Oxidative Phosphorylation														
Ndufb8	O09111	EPTMQWQEDPEPEDENVYAK [48–67]	14	4	1.00	0.79	14	4	1.00	1.01	73	7	1.00	1.13
Sdhb	Q9CQA3	DLVPDLSNFYAQYK [140–153]	74	16	1.00	0.70	76	16	1.00	0.96	227	20	1.00	1.24
Uqcrc2	Q9DB77	TSAAPGGVPLQPQDLEFTK [24–42]	94	21	1.00	0.84	107	22	1.00	1.19	324	26	1.00	1.41
Cox5a	P12787	IIDAALR [84–90]	5	2	1.00	0.84	9	4	1.00	1.02	57	10	1.00	1.04
Atp5a1	Q03265	GMSLNLEPDNVGVVVFGNDK [104–123]	333	37	1.00	0.92	409	40	1.00	1.11	654	43	1.00	1.52
Tfam	P40630	NLSPEEK [190–196]	11	6	1.00	1.62	13	7	1.00	0.96	35	12	1.00	0.99
Hspd1	P63038	DMAIATGGAVFGEEGLNLNLEDVQAHDLGK [315–344]	442	46	1.00	0.85	517	48	1.00	0.96	1758	58	1.00	1.11
Ucp1	P12242	GVLGTITTLAK [57–67]	6	3	1.00	1.59	ND	ND	ND	ND	626	21	1.00	2.67
Ucp3	P56501	FLGAGTAACFADLLTFPLDTAK [17–38]; GTMDAYR [157–163]	2	1	1.00	0.74	ND	ND	ND	ND	21	9	1.00	1.58

Shown are the fold changes in the proteins between the chow-fed WT and dox-fed **Tg-$^{AT\text{-}hA2}$;mA2$^{+/+}$** mice. The TMT-MS data was first normalized by total ion species for each sample, followed by a ratio of protein to cyclophilin. Shown is a representative unique peptide that was detected for each protein consistent for all three adipose depots, except for Cebpα and Ucp3, where 2 peptides are listed. The fold change shown for hAGPAT2 in dox-fed **Tg-$^{AT\text{-}hA2}$;mA2$^{+/+}$** mice is an approximate fold change, as the human Agpat2 transgene is not expressed in chow-fed WT mice. P-values are indicated with symbols where significant, determined using One-Way ANOVA. * - $p < 0.05$, ‡ - $p < 0.01$, $ - $p < 0.001$. PSM – peptide-spectrum match. AA – amino acid. ND – not detected. SubQ, subcutaneous adipose tissue; gonadal, gonadal adipose tissue; BAT, brown adipose tissue. **WT - Tg-$^{AT\text{-}hA2}$;mA2$^{+/+}$**, is abbreviated to **Tg-mA2$^{+/+}$**.

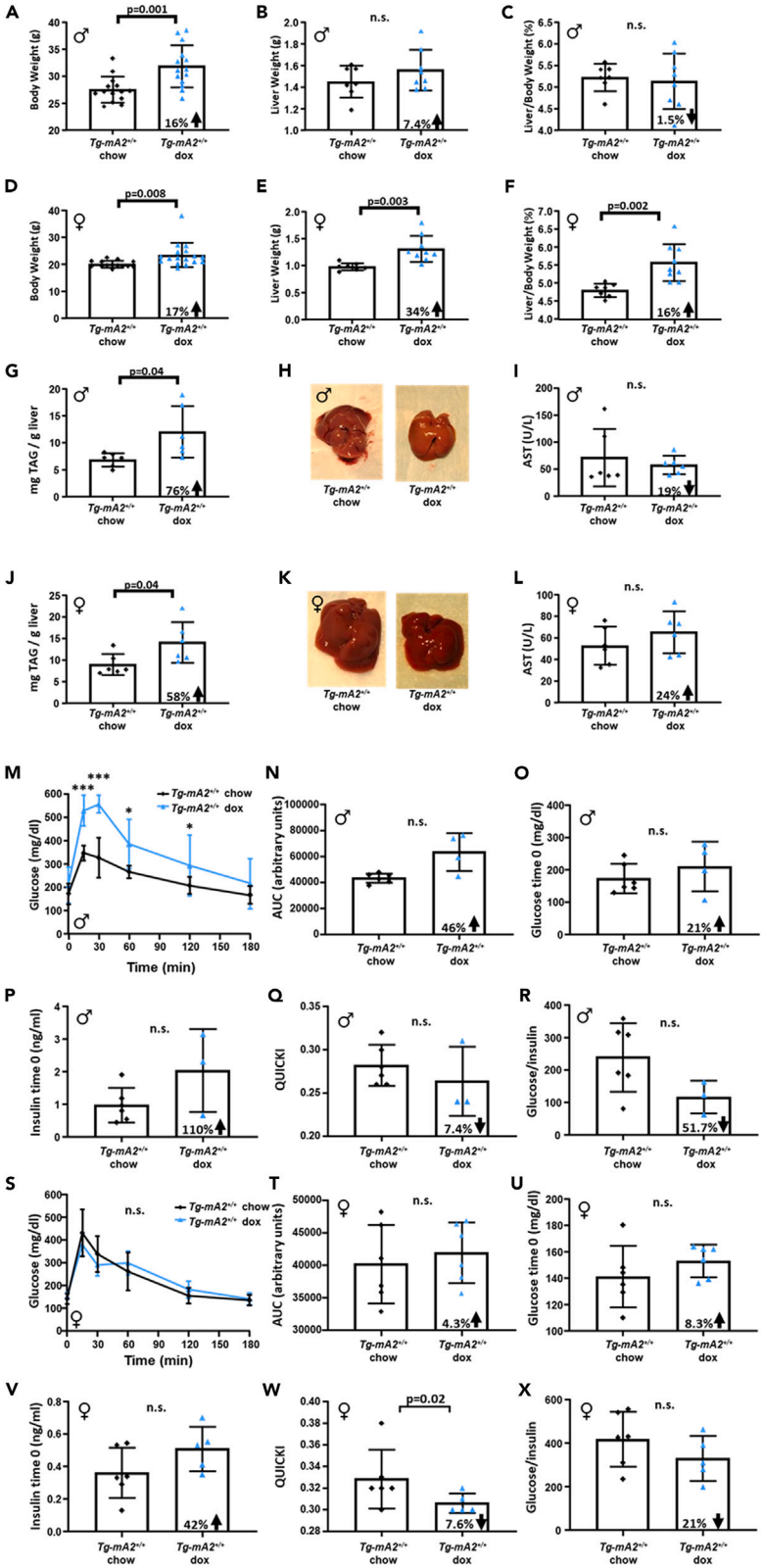
A
p=0.001
Body Weight (g)
16%
B
n.s.
Liver Weight (g)
7.4%
C
n.s.
Liver/Body Weight (%)
1.5%
D
p=0.008
Body Weight (g)
17%
E
p=0.003
Liver Weight (g)
34%
F
p=0.002
Liver/Body Weight (%)
16%
G
p=0.04
mg TAG / g liver
76%
H
I
n.s.
AST (U/L)
19%
J
p=0.04
mg TAG / g liver
58%
K
L
n.s.
AST (U/L)
24%
M
Glucose (mg/dl)
Time (min)
Tg-mA2+/+ chow
Tg-mA2+/+ dox
N
n.s.
AUC (arbitrary units)
46%
O
n.s.
Glucose time 0 (mg/dl)
21%
P
n.s.
Insulin time 0 (ng/ml)
110%
Q
n.s.
QUICKI
7.4%
R
n.s.
Glucose/insulin
51.7%
S
n.s.
Glucose (mg/dl)
Time (min)
T
n.s.
AUC (arbitrary units)
4.3%
U
n.s.
Glucose time 0 (mg/dl)
8.3%
V
n.s.
Insulin time 0 (ng/ml)
42%
W
p=0.02
QUICKI
7.6%
X
n.s.
Glucose/insulin
21%
Tg-mA2+/+ chow
Tg-mA2+/+ dox

Figure 4. Adipose tissue-specific expression of human AGPAT2 in Tg-$^{AT\text{-}hA2}$;$mA2^{+/+}$ mice results in a mild increase in liver triacylglycerol (TAG) but not liver dysfunction in 12 week old mice

Groups of Tg-$^{AT\text{-}hA2}$;$mA2^{+/+}$ mice were examined after 12 weeks of either chow or doxycycline (dox) diet for body and liver weight, liver triacylglycerol, and plasma aspartate aminotransferase (AST) levels. Glucose clearance was examined by oral glucose tolerance test (OGTT).

(A–F) The (A) male and (D) female body weight, (B) male and (E) female liver weight, and the (C) male and (F) female liver/body weight ratio are shown. The data are represented as mean ± SD. Each symbol represents individual measurements. Percent increase between chow-fed and dox-fed Tg-$^{AT\text{-}hA2}$;$mA2^{+/+}$ mice are shown in the bars. P-values were determined using the Student's *t* test.

(G and J) The liver TAG is increased in (G) male and (J) female dox-fed Tg-$^{AT\text{-}hA2}$;$mA2^{+/+}$ mice of both sexes. Each symbol represents individual measurements. Percent increase between chow-fed and dox-fed Tg-$^{AT\text{-}hA2}$;$mA2^{+/+}$ mice are shown in the bars. The data are represented as mean ± SD. P-values were determined using the Student's *t* test.

(H and K) The visual images of (H) male and (K) female liver excised at 12 weeks.

(I and L) Plasma AST levels in (I) male and (L) female mice remained unchanged. Each symbol represents individual mice. Percent increase or decrease between chow-fed and dox-fed Tg-$^{AT\text{-}hA2}$;$mA2^{+/+}$ mice are shown in the bars. The data are represented as mean ± SD. P-values were determined using the Student's *t* test.

(M and S) The glucose clearance in (M) male and (S) female chow- and doxycycline (dox)-fed Tg-$^{AT\text{-}hA2}$;$mA2^{+/+}$ mice at 12 weeks. The data are represented as mean ± SD. P-values were determined using mixed model repeated measurements. *$p < 0.05$, **$p < 0.001$.

(N and T) The same data points were used to generate the area under the curve ($AUC_{0\text{-}180}$) to determine the total glucose clearance in (N) males and (T) females. We note no significant difference in the AUC between chow- or dox-fed Tg-$^{AT\text{-}hA2}$;$mA2^{+/+}$ mice. P-values were determined using the Student's *t* test.

(O and U) The 6 h fasting plasma glucose levels in (O) males and (U) females.

(P and V) The 6 h fasting plasma insulin levels in (P) males and (V) females. Time 0 glucose and insulin levels show a mild but insignificant increase in dox-fed Tg-$^{AT\text{-}hA2}$;$mA2^{+/+}$ mice of both sexes. P-values were determined using the Student's *t* test.

(Q, R, W and X) QUICKI estimate in (Q) males and (W) females at time 0 indicates that the dox-fed Tg-$^{AT\text{-}hA2}$;$mA2^{+/+}$ mice have no significant change in insulin resistance, which is also reflected by the ratio of glucose/insulin at time 0 for (R) males and (X) females.

The data are represented as mean ± SD. Individual symbols represent independent mice. Percent increase or decrease between chow-fed and dox-fed Tg-$^{AT\text{-}hA2}$;$mA2^{+/+}$ mice are shown in the bars. P-values were determined using the Student's *t* test. n.s., not significant. Tg-$^{AT\text{-}hA2}$;$mA2^{+/+}$ abbreviated to Tg-$mA2^{+/+}$. See also Figures S5 and S6.

We followed the mice for an additional 12 weeks (a total of 24 weeks) to examine the development of glucose intolerance, insulin resistance, and liver TAG. Groups of chow- and dox-fed Tg-$^{AT\text{-}hA2}$;$mA2^{+/+}$ mice of both sexes were weighed at 24 weeks of age (Figures S5A and S5E). At 24 weeks, the body weight continued to be significantly increased in dox-fed Tg-$^{AT\text{-}hA2}$;$mA2^{+/+}$ mice compared to chow-fed Tg-$^{AT\text{-}hA2}$;$mA2^{+/+}$ mice, and the dox-fed Tg-$^{AT\text{-}hA2}$;$mA2^{+/+}$ mice livers continued to deteriorate in terms of hepatic steatosis. In dox-fed Tg-$^{AT\text{-}hA2}$;$mA2^{+/+}$ mice, the liver weight was significantly higher than chow-fed Tg-$^{AT\text{-}hA2}$;$mA2^{+/+}$ mice, but this only reached significance in males (Figures S5B and S5F), as did the liver/body weight ratio (Figures S5C and S5G). This increase in liver size can also be appreciated visually in Figure S5 (males I-J and females L-M). The liver TAG was significantly increased in male dox-fed Tg-$^{AT\text{-}hA2}$;$mA2^{+/+}$ mice compared to chow-fed Tg-$^{AT\text{-}hA2}$;$mA2^{+/+}$ mice, but not in females (Figures S5D and S5H). Furthermore, the AST levels of dox-fed Tg-$^{AT\text{-}hA2}$;$mA2^{+/+}$ mice were significantly elevated in both sexes (Figures S5K and S5N). The plasma triglyceride levels at 24 weeks were only increased in female dox-fed Tg-$^{AT\text{-}hA2}$;$mA2^{+/+}$ mice (Figures S5O and S5S) The plasma leptin, glucose, and insulin levels were all increased in dox-fed Tg-$^{AT\text{-}hA2}$;$mA2^{+/+}$ mice of both sexes, but only reached statistical significance for leptin and insulin in male mice (Figures S5P–S5R and S5T–S5V).

Increased adiposity in dox-fed Tg-$^{AT\text{-}hA2}$;$mA2^{+/+}$ mice results in a mild increase of liver triacylglycerol at 12 weeks

At 12 weeks of age, the dox-fed Tg-$^{AT\text{-}hA2}$;$mA2^{+/+}$ mice have increased body weight (Figures 4A and 4D), as noted before. Additionally, they have increased liver size in both sexes (Figures 4B and 4E), and an increased liver/body weight ratio (Figures 4C and 4E), but this only reached significance in female mice (Figures 4E and 4F). There is a mild increase in liver TAG in dox-fed mice of both sexes (Figures 4G and 4J), which is also reflected in the *ex situ* images of the whole liver (Figures 4H and 4K). Despite this mild increase in liver TAG, the liver function remains intact, as noted by no increase in the aspartate aminotransferase (AST) levels (Figures 4I and 4L). With an increase in adiposity in dox-fed Tg-$^{AT\text{-}hA2}$;$mA2^{+/+}$ mice, we would expect that the liver TAG would increase and result in liver dysfunction. However, we observed no difference compared to the chow-fed Tg-$^{AT\text{-}hA2}$;$mA2^{+/+}$ mice.

Measurement of key fatty acid, triacylglycerol synthesis, fatty acid oxidation, insulin signaling, and glucose metabolism transcripts in the livers of Tg-$^{AT\text{-}hA2}$;$mA2^{+/+}$ mice at 12 and 24 weeks

We measured the transcripts for key enzymes for several pathways involved in fatty acid and TAG synthesis, insulin and insulin-like factor signaling, and glucose metabolism, shown in Table 5. The expression of these key pathway-specific transcripts reflects the lack of a robust increase in liver TAG synthesis, except for the expression of *Mogat1*, which was increased 5-fold in male and 14-fold in female dox-fed Tg-$^{AT\text{-}hA2}$;$mA2^{+/+}$ mice compared to chow-fed Tg-$^{AT\text{-}hA2}$;$mA2^{+/+}$ mice. The increase in *Mogat1* in the livers of these mice is interesting, because previously we observed the increased expression of *Mogat1* in the context of $Agpat2^{-/-}$ lipodystrophic mice, where the fatty liver is more pronounced and the increased expression of *Mogat1* more than 40-fold.[3] Although, when we generated $Mogat1^{-/-}/Agpat2^{-/-}$ we could not decrease the liver TAG.[25] However, such a robust increase in *Mogat1* expression might have additional roles for this enzyme in the liver yet to be ascertained in both obese and lipodystrophic mice.

Table 5. RT-qPCR measurements of key genes for pathways of fatty acid and triacylglycerol synthesis, fatty acid oxidation, insulin signaling, and glucose metabolism in livers of 12 weeks chow- and doxycycline-fed Tg-$^{AT\text{-}hA2}$;m$A2^{+/+}$ mice

Sex	Male		Female	
Genotype	Tg-m$A2^{+/+}$		Tg-m$A2^{+/+}$	
Diet	Chow	Dox	Chow	Dox
samples pooled (n)	6	6	6	6
Gene	Fold	Fold ± SD	Fold	Fold ± SD
Fatty acid and TAG synthesis				
Acly	1.00	0.65 ± 0.00	1.00	1.32 ± 0.20
Acc1	1.00	0.81 ± 0.02	1.00	1.02 ± 0.04
Fas	1.00	0.77 ± 0.03	1.00	1.32 ± 0.01
Elovl6	1.00	1.06 ± 0.05	1.00	1.18 ± 0.01
Scd1	1.00	0.81 ± 0.10	1.00	1.19 ± 0.04
Scd2	1.00	0.70 ± 0.07	1.00	0.94 ± 0.09
Gpat1	1.00	1.01 ± 0.02	1.00	1.27 ± 0.03
mAgpat2	1.00	1.23 ± 0.02	1.00	1.46 ± 0.06
Ppap2c	1.00	0.74 ± 0.12	1.00	0.93 ± 0.01
Lipin 3	**1.00**	**0.84 ± 0.13**	**1.00**	**1.11 ± 0.08**
Dgat2	1.00	1.06 ± 0.06	1.00	1.33 ± 0.04
Mogat1	**1.00**	5.03 ± 0.09	**1.00**	13.82 ± 0.03
Pparγ	1.00	1.54 ± 0.17	1.00	1.67 ± 0.23
Fatty acid oxidation				
Pparα	1.00	0.96 ± 0.05	1.00	1.42 ± 0.12
Ucp2	1.00	0.80 ± 0.00	1.00	1.45 ± 0.00
SREBP pathway				
Srebp-1a	1.00	0.91 ± 0.04	1.00	1.20 ± 0.06
Srebp-1c	1.00	1.18 ± 0.08	1.00	1.82 ± 0.27
Insulin and IGF-1 signaling				
IR	1.00	0.79 ± 0.02	1.00	1.11 ± 0.10
Irs-1	1.00	0.72 ± 0.04	1.00	0.98 ± 0.17
Irs-2	1.00	0.70 ± 0.01	1.00	0.69 ± 0.03
Igf-1 R	**1.00**	**0.84 ± 0.20**	**1.00**	**1.25 ± 0.14**
Igf-1	1.00	0.93 ± 0.00	1.00	1.39 ± 0.01
IGF-bp	1.00	0.84 ± 0.02	1.00	0.78 ± 0.01
Glucose metabolism				
Chrebp	1.00	0.99 ± 0.02	1.00	0.84 ± 0.01
Pepck	1.00	0.87 ± 0.03	1.00	1.05 ± 0.25
G-6-Pase	1.00	1.19 ± 0.01	1.00	1.38 ± 0.06
PK	1.00	0.92 ± 0.02	1.00	1.33 ± 0.10

An equal quantity of total RNA was pooled from each mouse (n = 6) and quantified twice in duplicate. Data are shown as the average of 2 values compared to chow-fed Tg-$^{AT\text{-}hA2}$;m$A2^{+/+}$ mice = 1. Bold text indicates a raw C_t value >30. Wherever the raw C_t value >30, we consider the fold change as approximate. For the human transgene *hAGPAT2*, the raw C_t values are as follows: in males, chow-fed WT C_t = 31.26, dox-fed WT C_t = 31.33; in females, chow-fed WT C_t = 30.94, dox-fed WT C_t = 30.14. Tg-$^{AT\text{-}hA2}$;m$A2^{+/+}$ abbreviated to Tg-m$A2^{+/+}$.

We measured the transcripts for key enzymes in 12-week-old mice as well as in 24 weeks mice (Table S2). Compared to the expression of these key enzymes at 12 weeks (see Table 5), where we noted no significant change in dox-fed Tg-$^{AT\text{-}hA2}$;m$A2^{+/+}$ mice of either sex, at 24 weeks we observe an increase in the expression of many of the fatty acid and TAG synthesis enzymes in dox-fed Tg-$^{AT\text{-}hA2}$;m$A2^{+/+}$ mice. Most

notable was the increase in *Mogat1*, which increased 38-fold in males and 17.5-fold in females. Surprisingly, despite the fact that the fatty acid and TAG synthesis pathways are upregulated in dox-fed Tg-$^{AT\text{-}hA2}$;*mA2*$^{+/+}$ mice, the transcripts involved in the insulin and IGF-1 signaling pathways are not changed compared to chow-fed Tg-$^{AT\text{-}hA2}$;*mA2*$^{+/+}$ mice. While the insulin receptor and insulin receptor substrate transcripts are not increased, transcripts involved in the downstream pathway could be affected, which are not measured in this study (i.e., *Pip3k*). Increased expression of pyruvate kinase in the livers of dox-fed Tg-$^{AT\text{-}hA2}$;*mA2*$^{+/+}$ mice would indicate increased glycolysis, leading to increased substrates for lipid synthesis.

Fasting chow- and dox-fed Tg-$^{AT\text{-}hA2}$;mA2$^{+/+}$ mice have similar glucose disposal despite the increase in adiposity at 12 and 24 weeks

We have seen in non-fasting dox-fed Tg-$^{AT\text{-}hA2}$;*mA2*$^{+/+}$ mice that the plasma insulin levels are elevated (see Figures 3H and 3L). This prompted us to measure the glucose disposal of these mice using the oral glucose tolerance test (OGTT). We tested 12 week old mice of both sexes that were fasted for 6 h. A tail vein glucose measurement after a bolus of gavaged glucose measured for 0–180 min is shown in Figures 4M and 4S. While the glucose clearance seems to be similar in female chow- and dox-fed Tg-$^{AT\text{-}hA2}$;*mA2*$^{+/+}$ mice, male dox-fed Tg-$^{AT\text{-}hA2}$;*mA2*$^{+/+}$ mice have higher plasma glucose at 15–120 min. However, AUC remains statistically insignificant for both the sexes (Figures 4N and 4T). Measuring the ratio of fasting plasma glucose and insulin at time 0 is a good measure of insulin resistance (known as QUICKI). As shown in Figure 4, the fasting glucose (O, U) and insulin (P, V) levels in dox-fed Tg-$^{AT\text{-}hA2}$;*mA2*$^{+/+}$ mice were slightly elevated compared to chow-fed Tg-$^{AT\text{-}hA2}$;*mA2*$^{+/+}$ mice in both sexes, but this did not reach statistical significance. However, the QUICKI measurement did reach significance between the female chow-fed and dox-fed Tg-$^{AT\text{-}hA2}$;*mA2*$^{+/+}$ mice (Figure 4W). While there was a decreasing trend in male dox-fed Tg-$^{AT\text{-}hA2}$;*mA2*$^{+/+}$ mice compared to chow-fed Tg-$^{AT\text{-}hA2}$;*mA2*$^{+/+}$ mice, it did not reach statistical significance (Figure 4Q). Another way to interpret insulin resistance is to analyze the ratio of glucose/insulin at time 0. Based on this, neither male nor female dox-fed Tg-$^{AT\text{-}hA2}$;*mA2*$^{+/+}$ mice reach a statistically significant decrease in the glucose/insulin ratio (Figures 4R and 4X).

We repeated the OGTT in chow-fed and dox-fed Tg-$^{AT\text{-}hA2}$;*mA2*$^{+/+}$ mice of both sexes after 24 weeks (Figures S6A and S6G). While the tail vein glucose measurements are similar in chow- and dox-fed Tg-$^{AT\text{-}hA2}$;*mA2*$^{+/+}$ mice, dox-fed Tg-$^{AT\text{-}hA2}$;*mA2*$^{+/+}$ mice of both sexes have higher plasma glucose after the oral glucose bolus and do not quite return to the base line, but this only reached statistical significance in male mice. Additionally, the AUC is significantly increased in the dox-fed Tg-$^{AT\text{-}hA2}$;*mA2*$^{+/+}$ mice only in the male mice (Figures S6B and S6H). While the fasting glucose is not significantly different between chow- and dox-fed Tg-$^{AT\text{-}hA2}$;*mA2*$^{+/+}$ mice of both sexes (Figures S6C and S6I), the fasting insulin is elevated in dox-fed Tg-$^{AT\text{-}hA2}$;*mA2*$^{+/+}$ mice of both sexes, but this only reached significance in male mice (Figures S6D and S6J). However, the QUICKI measurement did show a significant decrease in dox-fed Tg-$^{AT\text{-}hA2}$;*mA2*$^{+/+}$ mice of both sexes compared to chow-fed Tg-$^{AT\text{-}hA2}$;*mA2*$^{+/+}$ mice (Figures S6E and S6K), indicating some level of insulin resistance. The ratio of glucose/insulin at time 0 was also decreased in dox-fed Tg-$^{AT\text{-}hA2}$;*mA2*$^{+/+}$ mice compared to chow-fed Tg-$^{AT\text{-}hA2}$;*mA2*$^{+/+}$ mice, but was only significant in male mice (Figures S6F and S6L).

Indirect calorimetric measurement in 12 weeks chow- and dox-fed Tg-$^{AT\text{-}hA2}$;mA2$^{+/+}$ mice of both sexes

To comprehensively assess the energy regulation in the chow-fed and dox-fed Tg-$^{AT\text{-}hA2}$;*mA2*$^{+/+}$ mice, we measured the food and water intake, O_2 and CO_2, and computed basal energy expenditure (EE), energy balance, and respiratory exchange ratio (RER) in these mice using indirect calorimetry methods.[26,27] As expected, due to the observed increase in body weight, dox-fed Tg-$^{AT\text{-}hA2}$;*mA2*$^{+/+}$ mice consume more food than chow-fed Tg-$^{AT\text{-}hA2}$;*mA2*$^{+/+}$ mice (Figures 5A and 5B; Figures S7A–S7D), but there is no increase in water intake (Figures 5C and 5D; Figures S7E–S7H). Additionally, we note the RER, a measure of fuel switching between fat and carbohydrate, does not vary between the chow and dox-fed Tg-$^{AT\text{-}hA2}$;*mA2*$^{+/+}$ mice during the light periods, but they do differ from chow-fed WT mice, mainly during the dark cycle for both sexes, mostly the period when the mice eat (Figures 5E and 5F). During the first 48 h, the dox-fed mice show a greater difference in RER during the dark cycles than the chow-fed mice, but these differences are lost at prolonged measurements. An RER near 0.7 indicates that fat is the predominant fuel source, while a value of 1.0 is indicative of carbohydrates. A value between 0.7 and 1.0 suggests a mix of both fat and carbohydrates. While the chow-fed WT mice switch their fuel source between fat and carbohydrates, as expected, the dox-fed Tg-$^{AT\text{-}hA2}$;*mA2*$^{+/+}$ mice maintain an RER around 0.8 throughout the duration of the experiment, reflecting a constant use of a mix of both fat and carbohydrates.

The concept of energy balance pertains to the balance of energy intake versus energy expenditure.[28] If the energy intake and expenditure are equal, the energy balance reaches close to zero. However, when the energy expenditure is greater than the energy intake, the energy balance is negative. This energy balance is dependent on a number of factors, including the animals' ambulatory activity, body mass, and food intake. The locomotor and ambulatory activity of these mice showed no statistically significant difference between any of the three groups of mice (Figures S7I–S7L). When compared to chow-fed Tg-$^{AT\text{-}hA2}$;*mA2*$^{+/+}$ mice, the energy expenditure of the dox-fed Tg-$^{AT\text{-}hA2}$;*mA2*$^{+/+}$ mice was mildly increased, but only in females (Figures 5G and 5H; Figures S7M and S7N). The energy balance can be calculated by [Energy Balance = food intake – energy expenditure]. Based on this, the dox-fed Tg-$^{AT\text{-}hA2}$;*mA2*$^{+/+}$ mice had a larger positive cumulative energy balance compared to chow-fed Tg-$^{AT\text{-}hA2}$;*mA2*$^{+/+}$ mice in both sexes (Figures 5I and 5J; Figures S7O and S7P), which reflects that the dox-fed Tg-$^{AT\text{-}hA2}$;*mA2*$^{+/+}$ mice consume more calories but their energy expenditure remains similar to chow-fed Tg-$^{AT\text{-}hA2}$;*mA2*$^{+/+}$ mice. The regression analysis displayed in Figures 5K and 5L shows the relationship between EE and body mass; as the body mass increases, the energy expenditure should also increase. The relationship between energy expenditure and body mass is different between males and females in our study. For the males, both groups show a positive relationship; as the body mass increases, the energy expenditure goes up.

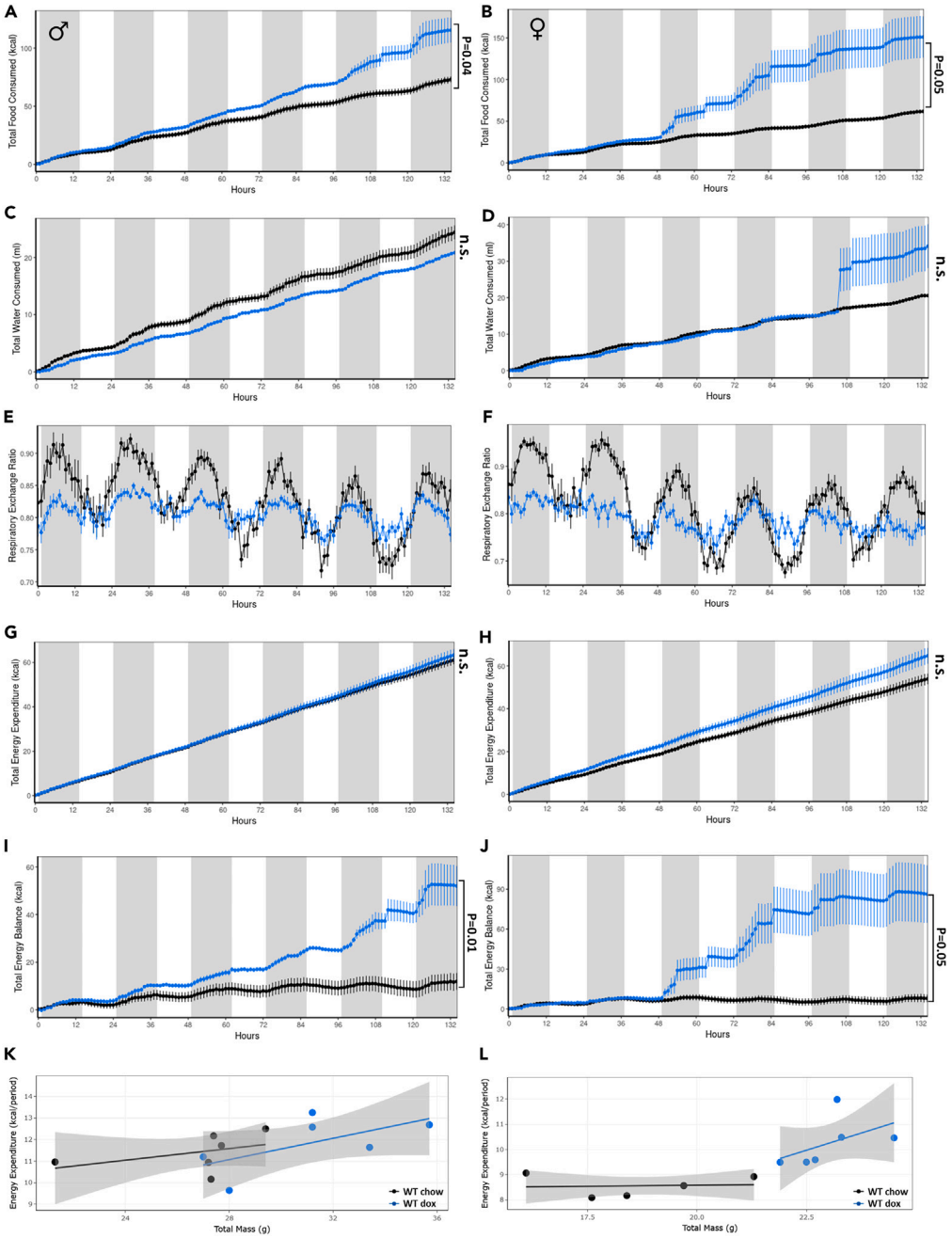

Figure 5. Indirect calorimetric measurements for chow and doxycycline (dox)-fed Tg-$^{AT\text{-}hA2}$;*mA2*$^{+/+}$ mice

(A and B) Cumulative food intake over 5 days for (A) males and (B) females.

(C and D) Cumulative water intake over 5 days for (C) males and (D) females.

(E and F) Respiratory exchange ratio (RER) over 5 days for (E) males and (F) females. Note that while chow-fed Tg-$^{AT\text{-}hA2}$;*mA2*$^{+/+}$ mice switch between the fuel source (carbohydrates at night and fat during the day), the dox-fed Tg-$^{AT\text{-}hA2}$;*mA2*$^{+/+}$ mice are more consistently utilizing a mix of carbohydrates and fat.

(G and H) The resting total energy expenditure (TEE) in (G) males and (H) females show increased TEE in dox-fed Tg-$^{AT\text{-}hA2}$;*mA2*$^{+/+}$ mice compared to chow fed mice, but this relationship was found only in female mice.

(I and J) Total cumulative energy balance (TEB) over 5 days in (I) males and (J) females. Dox-fed Tg-$^{AT\text{-}hA2}$;*mA2*$^{+/+}$ mice show positive TEB compared to chow-fed Tg-$^{AT\text{-}hA2}$;*mA2*$^{+/+}$ mice.

(K and L) The generalized linear model (GLM) regression lines are plotted as the resting energy expenditure against the total body mass in (K) males and (L) females, which shows an increase in energy expenditure upon increase in body weight. Dark hours are shaded in gray, light hours are in white. All measurements are tabulated for total body weight, see text for explanation. N = 6 per group. The data was analyzed using CalR, a web-based analysis tool for indirect calorimetry experiments. The panels are screenshots obtained from CalR. P-values for panels A-J were determined using the Student's *t* test. For additional statistics calculated in the CalR program, see Figure S8B. Tg-$^{AT\text{-}hA2}$;*mA2*$^{+/+}$ abbreviated to Tg-*mA2*$^{+/+}$. See also Figure S6.

Table 6. RT-qPCR measurements of select genes for mitochondrial oxidative phosphorylation (OXPHOS) in adipose tissue depots of 12 and 24 weeks chow-fed WT and doxycycline (dox)-fed Tg-$^{AT\text{-}hA2}$;m$A2^{+/+}$ mice

Duration	12 weeks				24 weeks			
Genotype	Tg-m$A2^{+/+}$							
Sex	Male		Female		Male		Female	
Diet	Chow	Dox	Chow	Dox	Chow	Dox	Chow	Dox
Tissue	**SubQ**							
Samples pooled (n)	4	4	4	4	3	4	5	6
Ndufb8	1.00	0.22	1.00	0.31	**1.00**	0.86	1.00	0.68
Sdhb	1.00	0.29	1.00	0.34	1.00	0.62	1.00	2.00
Uqcrc2	1.00	0.32	1.00	0.35	1.00	0.76	1.00	0.70
Cox5a	1.00	0.38	1.00	0.50	1.00	0.48	1.00	2.17
Atp5a1	1.00	0.43	1.00	0.42	1.00	0.54	1.00	0.80
Tfam	1.00	0.87	1.00	2.04	1.00	0.62	1.00	0.82
Hspd1	1.00	0.45	1.00	1.33	1.00	0.66	1.00	0.96
Ucp1	1.00	0.04	1.00	**0.00**	1.00	0.03	1.00	**0.02**
Ucp2	1.00	1.29	1.00	1.08	1.00	1.85	1.00	1.22
Ucp3	1.00	0.19	1.00	0.16	1.00	0.62	1.00	0.26
Tissue	**Gonadal**							
Samples pooled (n)	3	4	4	4	3	4	5	6
Ndufb8	1.00	0.52	1.00	0.43	1.00	0.23	1.00	**0.25**
Sdhb	1.00	0.59	1.00	0.65	1.00	0.48	1.00	0.24
Uqcrc2	1.00	0.62	1.00	0.47	1.00	0.31	1.00	0.37
Cox5a	1.00	0.87	1.00	0.81	1.00	0.53	1.00	0.33
Atp5a1	1.00	0.70	1.00	0.58	1.00	0.43	1.00	0.29
Tfam	1.00	0.64	1.00	0.63	1.00	0.57	1.00	1.02
Hspd1	1.00	0.67	1.00	0.54	1.00	0.50	1.00	0.71
Ucp1	**1.00**	**1.71**	1.00	0.03	1.00	0.05	1.00	0.54
Ucp2	1.00	1.59	1.00	1.43	1.00	3.59	1.00	2.80
Ucp3	1.00	1.21	1.00	0.34	1.00	0.19	1.00	0.90
Tissue	**BAT**							
Samples pooled (n)	4	4	4	4	3	4	5	6
Ndufb8	1.00	0.65	1.00	0.93	1.00	0.46	1.00	1.25
Sdhb	1.00	0.70	1.00	0.78	1.00	0.33	1.00	0.67
Uqcrc2	1.00	0.85	1.00	1.11	1.00	0.45	1.00	1.38
Cox5a	1.00	0.56	1.00	0.66	1.00	0.39	1.00	0.66
Atp5a1	1.00	0.65	1.00	0.83	1.00	0.34	1.00	1.05
Tfam	1.00	0.52	1.00	0.49	1.00	0.54	1.00	0.99
Hspd1	1.00	0.51	1.00	0.61	1.00	0.64	1.00	1.45
Ucp1	1.00	0.58	1.00	0.68	1.00	0.25	1.00	1.11
Ucp2	1.00	1.84	1.00	2.21	1.00	3.69	1.00	1.60
Ucp3	1.00	0.67	1.00	0.67	1.00	0.35	1.00	0.99

An equal quantity of total RNA was pooled from each mouse (n = 3–6) and quantified once in duplicate. Data are shown compared to chow-fed WT mice = 1. Bold text indicates a raw C_t value >30. Wherever the raw C_t value >30, we consider the fold change as approximate. SubQ, subcutaneous adipose tissue; gonadal, gonadal adipose tissue; BAT, brown adipose tissue. **WT - Tg-$^{AT\text{-}hA2}$;m$A^{+/+}$** is abbreviated to **Tg-m$A2^{+/+}$**.

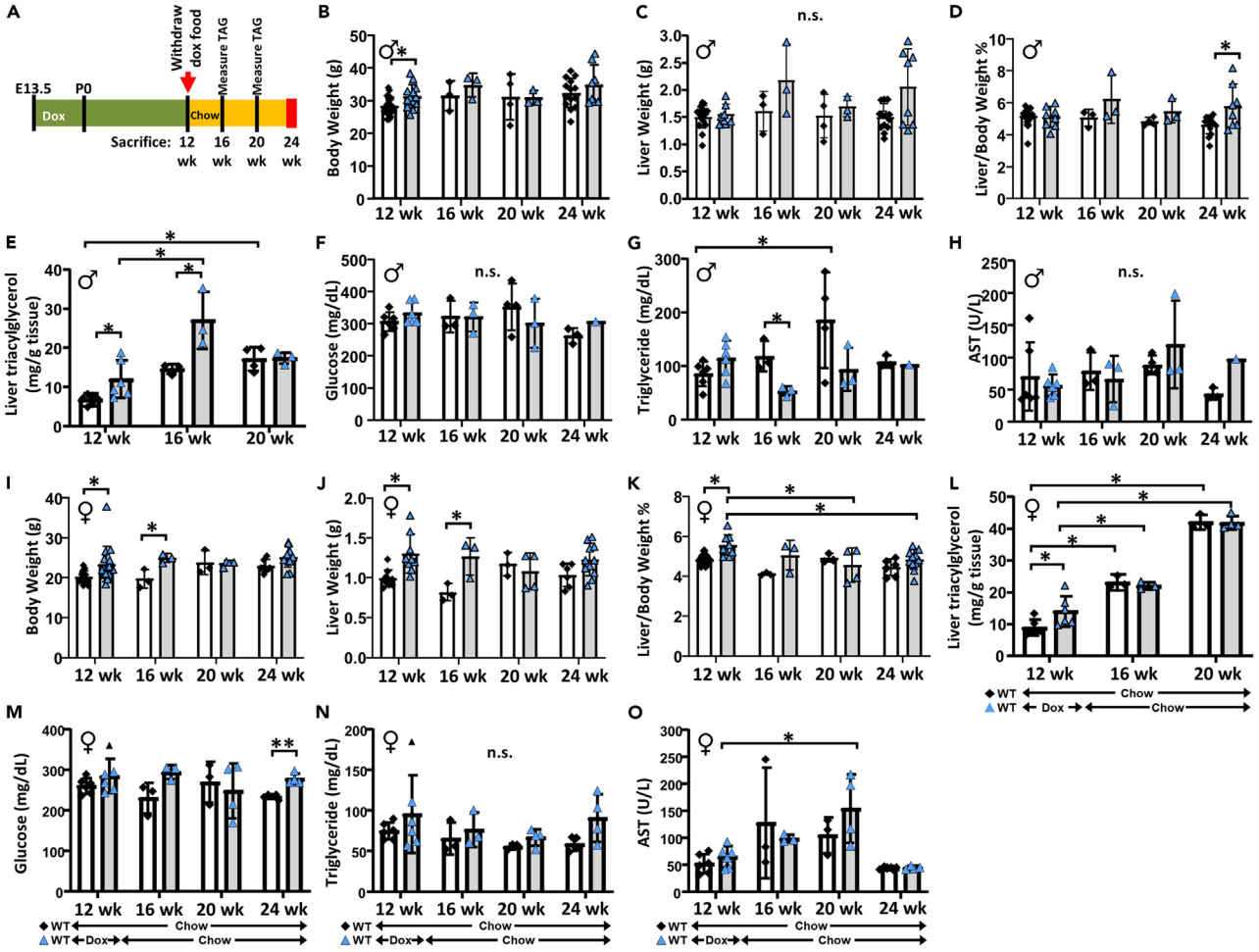

Figure 6. Turning on hAGPAT2 transgene in adipose tissue of Tg-$^{AT\text{-}hA2}$;$mA2^{+/+}$ mice for 12 weeks, followed by its removal (turning off hAGPAT2 expression), did not result in any significant changes in liver function

(A) The strategy for dox-fed Tg-$^{AT\text{-}hA2}$;$mA2^{+/+}$ mice with subsequent removal (to turn off hAGPAT2 expression in adipose tissue(AT)).

(B–O) Shown are the (B) male and (I) female body weight, (C) male and (J) female liver weight, (D) male and (K) female liver/body ratio, (E) male and (L) female liver triacylglycerol, (F) male and (M) female plasma glucose, (G) male and (N) female plasma triglycerides, and (H) male and (O) female plasma aspartate aminotransferase (AST) at the various time points. Despite turning off the hAGPAT2 overexpression, the liver weight in dox-fed Tg-$^{AT\text{-}hA2}$;$mA2^{+/+}$ females remained significantly higher than chow-fed Tg-$^{AT\text{-}hA2}$;$mA2^{+/+}$ mice for 4 weeks after dox removal, although this returned to normal levels by 8 weeks dox removal (panel J). Nevertheless, the plasma AST, an indicator of liver dysfunction, remained unchanged (panel O). This indicates the overexpression of hAGPAT2 in AT does not affect the liver function. The data are represented as mean ± SD. Individual values are shown. Statistics were determined using Student's *t* test (for chow-fed vs. dox-fed comparison) or two-way ANOVA (for all other comparisons). *p < 0.05, **p < 0.001. n.s., not significant. Tg-$^{AT\text{-}hA2}$;$mA2^{+/+}$ abbreviated to Tg-$mA2^{+/+}$.

However, the female chow-fed WT mice have a flat slope (i.e., as the body mass increases, the energy expenditure does not increase), while the dox-fed Tg-$^{AT\text{-}hA2}$;$mA2^{+/+}$ mice have a positive energy slope.

As mentioned above, one way the animals regulate their energy balance is by thermogenesis. We therefore measured a few of the key enzymes for mitochondrial oxidative phosphorylation (OXPHOS) and uncoupling protein (*Ucp1-3*) in the three AT depots. There are multiple proteins in each of the five complexes, cI-cV, that form the electron transport chain (ETC).[29,30] We selected key markers for each of these complexes and a mitochondrial specific transcription factor. We note no increase in the mRNA expression of these enzymes and *Ucp1* at 12 and 24 weeks (Table 6), thus eliminating the possibility of increased thermogenesis in regulating or dissipating energy. Studies now suggest several additional mechanisms independent of *Ucp1* for energy regulation/dissipation. These include creatine, lipid, calcium cycling or *Ucp1* independent pathway driven by the ADP/ATP carrier (AAC) reviewed in.[31] However, *Ucp2* was increased 1.5– to 2-fold in the three adipose depots examined in both male and female mice at 12 weeks, while it was increased 2.8– to 3.7-fold in both male and female gonadal tissue, and in male BAT, but not female BAT or SubQ of both sexes at 24 weeks, although its role in thermogenesis is unclear.

Turning off the expression of hAGPAT2 in adipose tissue results in the normalization of liver function

In these experiments, we initially fed groups of Tg-$^{AT\text{-}hA2}$;*mA2*$^{+/+}$ mice of both sexes with either chow or dox food for 12 weeks. We then removed the dox food and substituted with a chow diet for a further 12 weeks and examined the mice at 4 week intervals post-dox food removal (schematic Figure 6A). We expected that upon removal of dox food (i.e., turning off the expression of *hAGPAT2*), the dox-fed Tg-$^{AT\text{-}hA2}$;*mA2*$^{+/+}$ mice would return to a more chow-fed phenotype, which is what we observed. In Figure 6B, I, the body weight of the dox-fed Tg-$^{AT\text{-}hA2}$;*mA2*$^{+/+}$ mice returned to chow-fed levels by week 20 (8 weeks post dox food removal). The liver weight also returned to chow-fed levels, as did the ratio of liver/body weight (Figures 6C and 6D, 6J and 6K). The liver TAG did increase in both male and female dox-fed Tg-$^{AT\text{-}hA2}$;*mA2*$^{+/+}$ mice at 12 weeks, and only in males at 16 weeks, but not at 20 weeks (Figures 6E and 6L). The non-fasting glucose levels were similar between chow-fed and dox-fed at all time points in both sexes, except at 24 weeks in female mice, where the glucose levels were slightly increased in dox-fed Tg-$^{AT\text{-}hA2}$;*mA2*$^{+/+}$ mice compared to chow-fed Tg-$^{AT\text{-}hA2}$;*mA2*$^{+/+}$ mice (Figures 6F and 6M). The plasma triglyceride levels of dox-fed Tg-$^{AT\text{-}hA2}$;*mA2*$^{+/+}$ mice also returned to chow-fed levels (Figures 6G and 6N). We did see a slight increase in AST levels of dox-fed Tg-$^{AT\text{-}hA2}$;*mA2*$^{+/+}$ mice after 12 weeks of dox removal (Figures 6H and 6O). Otherwise, the AST levels remained at chow-fed levels. In this study, we did not specifically monitor the loss of AT upon dox food removal, since the focus was on liver function, so we cannot say if there was a decrease in AT upon turning off the expression of h*AGPAT2* in AT.

DISCUSSION

Since discovering the *AGPAT2* biallelic pathogenic variants in patients with congenital generalized lipodystrophy, type 1[2] and generating the Agpat2-deficient mouse model of generalized lipodystrophy,[3] the lack of AT has precluded us from studying the role of *Agpat2* in the biology of adipose tissue. The new murine model of regulated adipose tissue-specific expression of *Agpat2* allows us to study the role of *Agpat2* in the biology of AT[4] (the role of this enzyme in hepatic steatosis to be presented in this journal or elsewhere). Additionally, we studied the role of leptin in a liver-specific leptin-deficient mouse on the *Agpat2*$^{-/-}$ genetic background, which reduced hepatic steatosis, confirming leptin's central role in regulating hepatic fat.[32] If *de novo* lipogenesis and TAG synthesis pathway gene expression is decreasing in AT, why is the AT increasing? One possible explanation is hyperplasia (cell multiplication), as opposed to cell hypertrophy (increase in cell size). In this study, we show that the role of *Agpat2* in AT is not in synthesizing TAG, but in synthesizing primarily phospholipids, which are also signaling molecules and thus likely aid in generating more adipocytes either by enhancing preadipocyte differentiation to adipocytes or in generating preadipocytes from the mesenchymal cell pool.

This argument is made because cellular TAG can also be synthesized via alternative pathways (see Figure S8A). In the monoacylglycerol (MAG) pathway, monoacylglycerol (MAG) is converted to diacylglycerol (DAG), and then to TAG. The utilization of this pathway has been suggested before based on the fact that the livers of A*gpat2*$^{-/-}$ lipodystrophic mice showed several-fold increase in *Mogat1* expression, both at mRNA and protein levels.[3] However, if *Mogat1* was able to compensate for the loss of TAG synthesis via the *Agpat2* pathway, the A*gpat2*$^{-/-}$ mice[3] should have shown TAG-filled adipocytes via the MAG pathway. Additionally, upon generating a double *Agpat2*$^{-/-}$/*Mogat1*$^{-/-}$ mouse,[25] we did not observe any decrease in liver TAG, further confirming that *Mogat1* is not critical for synthesizing TAG in the liver. We believe this is due to decreased PA synthesis in AT. In one report, the levels of PA in yeast are ~3% of the total phospholipids.[33] In fact, the cellular PAs are difficult to measure because of multiple degrading enzymes in play, such as phospholipase D (PLD), diacylglycerol kinases (DGKs) and phosphatidic acid phosphatases (PAP) as reviewed by Kim and Wang.[34] Such a low level of cellular PAs further supports their role as signaling molecules. In addition to the MAG pathway, the Choline-Phosphatidylcholine pathway (abbreviated as C-PC) can bypass the other pathways described above to use choline as the initial substrate. In this pathway, phosphatidylcholine (PC) is converted to DAG and on to TAG. In the absence of the *Agpat2* pathway in AT, the MAG and C-PC pathways could have been utilized to synthesize TAG, which we do not observe. This strongly suggests that the role of *Agpat2* is to generate molecular species of PA, which very specifically help in differentiating the mesenchymal cells from preadipocytes and/or preadipocytes from adipocytes.

Consistent with this, we noted that AT obtained from mice overexpressing h*AGPAT2* had decreased expression of *de novo* lipogenesis transcripts, and no increase in the expression of *Mogat1*. Therefore, it is unlikely that the MAG pathway is involved in synthesizing TAGs. However, we do see an increase in *Mogat2* transcript expression, but only in white AT known to synthesize TAG (SubQ and gonadal), as opposed to BAT, which is thermogenic in nature. *Mogat2* is mainly expressed in enterocytes, where its role is well defined.[35,36] A recent study using a cellular model for the liver, HepG2 cells, showed a mild effect in TAG synthesis, but only upon exogenously providing oleic acid in culture media.[37] The role of *Mogat2* in adipocytes has not been studied. This further substantiates the idea that overexpressing *AGPAT2* in AT increases adipocyte hyperplasia, but not TAG synthesis, likely from the differentiation of mesenchymal cells to preadipocytes and/or preadipocytes to adipocytes.

In this study, we also observed that the increase in AT mass did not result in any significant liver or metabolic dysfunction, at least through 24 weeks of AT-specific overexpression of h*AGPAT2*. While the livers of these mice did have a slight increase in TAG, consistent with a slight increase in plasma AST levels, the OGTT did not reveal insulin resistance. This substantiates the established norm that an increase in AT selectively stores the fat in adipocytes, protecting other peripheral tissues. A more severe liver or metabolic dysfunction may develop if the mice are followed for a longer period while continuing to overexpress hAGPAT2 in the AT when lipid overload in adipocytes results in their dysfunction.

In the current study, we overexpressed the h*AGPAT2* enzyme from embryonic day 13.5, the earliest reported detection of adipocytes. A limitation of this study is that *AGPAT2* is overexpressed embryonically, which could affect cells of the adipose lineage(s) to be adversely imprinted. In the future, murine models can be developed to ascertain the embryonic expression of *Agpat2* by using a reporter gene

(β-galactosidase, green fluorescence protein (GFP), luciferase, and so forth) expressed using the endogenous *Agpat2* promoter. Although there are some available murine models for ascertaining preadipocytes, these models have been generated based on the biology of the differentiation of committed preadipocytes into adipocytes. Using the lipodystrophic mouse model will certainly shed more light on adipocyte lineage tracing.

Based on our study that *Agpat2* has some role in differentiating adipocytes, a partial inhibition of this protein should result in reduced adipogenesis. This partial inhibition concept can be studied in $Agpat2^{+/-}$ (heterozygous) mice. Future studies using this heterozygous model will facilitate investigation into how AT responds to a high fat diet; will the $Agpat2^{+/-}$ mice develop anomalies or be protected from excessive energy intake?

Limitations of the study

A limitation of this study is that the over-expression of human AGPAT2 is only in adipose tissues in the $Agpat2^{+/+}$ mice, while endogenous AGPAT2 is expressed also in other tissues such as the liver, pancreas, and to low levels in the breast. This study, although not designed for this purpose, will not capture the contribution of endogenous AGPAT2 to the cross-tissue effect(s).

STAR★METHODS

Detailed methods are provided in the online version of this paper and include the following:

- KEY RESOURCES TABLE
- RESOURCE AVAILABILITY
  - Lead contact
  - Materials availability
  - Data and code availability
- EXPERIMENTAL MODEL AND STUDY PARTICIPANT DETAILS
  - Brief description of generation of Tg-$^{AT\text{-}hA2}$;$mA2^{+/+}$ mice
  - Oral glucose tolerance test (OGTT)
  - Indirect calorimetry
  - Plasma metabolite measurements
  - Total RNA isolation
  - Reverse transcription quantitative polymerase chain reaction (RT-qPCR)
  - Quantitative PCR using pooled sample strategy
  - Triacylglycerol assay
  - Magnetic resonance imaging and spectrometry
  - Nuclear magnetic resonance
  - Lipid mass spectrometry
  - Plasma leptin and insulin measurements
  - Tandem Mass Tag-mass spectrometry (TMT-MS) for adipose tissue
  - Histological analysis
  - Statistical analysis

SUPPLEMENTAL INFORMATION

Supplemental information can be found online at https://doi.org/10.1016/j.isci.2023.108653.

ACKNOWLEDGMENTS

The authors thank members of the mouse metabolic core at University of Texas Southwestern Medical Center for indirect calorimetric assays, William Bernard and Alexander Banks at Harvard Medical School, Boston, MA for their assistance with the CalR program. The UTSW Proteomics Core for assistance with targeted protein measurements. John Shelton, along with the members of the histopathology core, for the staining of adipose tissue samples. Taconic Biosciences for determining the mouse genetic background. National Institutes of Health R01- DK105448, 1P30DK127984, UL1TR003163, and P01HL160487 and the Southwestern Medical Foundation supported this work. The content is solely the responsibility of the authors and does not necessarily represent the official views of the National Institutes of Health.

AUTHOR CONTRIBUTIONS

AKA designed, supervised, helped collect data, analyzed the data, and wrote the first draft. KT collected most of the data, prepared figures, and copyedited the manuscript. JGM and GV provided the targeted lipid data. XL carried out additional statistical analysis. JDH and AG reviewed the manuscript and provided comments. All authors reviewed and edited the manuscript.

DECLARATION OF INTERESTS

The authors declare that they have no conflicts of interest in the contents of this article.

Received: February 21, 2023
Revised: July 11, 2023
Accepted: December 4, 2023
Published: December 7, 2023

REFERENCES

1. Agarwal, A.K. (2012). Lysophospholipid acyltransferases: 1-acylglycerol-3-phosphate O-acyltransferases. From discovery to disease. Curr. Opin. Lipidol. *23*, 290–302.
2. Agarwal, A.K., Arioglu, E., De Almeida, S., Akkoc, N., Taylor, S.I., Bowcock, A.M., Barnes, R.I., and Garg, A. (2002). AGPAT2 is mutated in congenital generalized lipodystrophy linked to chromosome 9q34. Nat. Genet. *31*, 21–23.
3. Cortes, V.A., Curtis, D.E., Sukumaran, S., Shao, X., Parameswara, V., Rashid, S., Smith, A.R., Ren, J., Esser, V., Hammer, R.E., et al. (2009). Molecular mechanisms of hepatic steatosis and insulin resistance in the AGPAT2-deficient mouse model of congenital generalized lipodystrophy. Cell Metab *9*, 165–176.
4. Agarwal, A.K., Tunison, K., Vale, G., McDonald, J.G., Li, X., Scherer, P.E., Horton, J.D., and Garg, A. (2023). Regulated adipose tissue-specific expression of human AGPAT2 in lipodystrophic Agpat2-null mice results in regeneration of adipose tissue. iScience *26*, 107806.
5. Sun, K., Wernstedt Asterholm, I., Kusminski, C.M., Bueno, A.C., Wang, Z.V., Pollard, J.W., Brekken, R.A., and Scherer, P.E. (2012). Dichotomous effects of VEGF-A on adipose tissue dysfunction. Proc Natl Acad Sci USA *109*, 5874–5879.
6. Angelakis, E., Merhej, V., and Raoult, D. (2013). Related actions of probiotics and antibiotics on gut microbiota and weight modification. Lancet Infect. Dis. *13*, 889–899.
7. Angelakis, E., Million, M., Kankoe, S., Lagier, J.C., Armougom, F., Giorgi, R., and Raoult, D. (2014). Abnormal weight gain and gut microbiota modifications are side effects of long-term doxycycline and hydroxychloroquine treatment. Antimicrob. Agents Chemother. *58*, 3342–3347.
8. Schwartz, B.S., Pollak, J., Bailey-Davis, L., Hirsch, A.G., Cosgrove, S.E., Nau, C., Kress, A.M., Glass, T.A., and Bandeen-Roche, K. (2016). Antibiotic use and childhood body mass index trajectory. Int. J. Obes. *40*, 615–621.
9. Weisberg, S.P., McCann, D., Desai, M., Rosenbaum, M., Leibel, R.L., and Ferrante, A.W., Jr. (2003). Obesity is associated with macrophage accumulation in adipose tissue. J. Clin. Invest. *112*, 1796–1808.
10. Wen, J., and Wang, L. (2022). Identification of key genes and their association with immune infiltration in adipose tissue of obese patients: a bioinformatic analysis. Adipocyte *11*, 401–412.
11. Wernstedt Asterholm, I., Tao, C., Morley, T.S., Wang, Q.A., Delgado-Lopez, F., Wang, Z.V., and Scherer, P.E. (2014). Adipocyte inflammation is essential for healthy adipose tissue expansion and remodeling. Cell Metab *20*, 103–118.
12. Zhu, Z., Guo, L., Yeltai, N., Xu, H., and Zhang, Y. (2022). Chemokine (C-C motif) ligand 2-enhanced adipogenesis and angiogenesis of human adipose-derived stem cell and human umbilical vein endothelial cell co-culture system in adipose tissue engineering. J Tissue Eng. Regen. Med. *16*, 163–176.
13. Hubscher, U., Maga, G., and Spadari, S. (2002). Eukaryotic DNA polymerases. Annu. Rev. Biochem. *71*, 133–163.
14. Lange, S.S., Takata, K., and Wood, R.D. (2011). DNA polymerases and cancer. Nat. Rev. Cancer *11*, 96–110.
15. Guilliam, T.A., and Yeeles, J.T.P. (2020). An updated perspective on the polymerase division of labor during eukaryotic DNA replication. Crit. Rev. Biochem. Mol. Biol. *55*, 469–481.
16. Frick, D.N., and Richardson, C.C. (2001). DNA primases. Annu. Rev. Biochem. *70*, 39–80.
17. Wang, Q.A., and Scherer, P.E. (2014). The AdipoChaser mouse: A model tracking adipogenesis in vivo. Adipocyte *3*, 146–150.
18. Zatulovskiy, E., and Skotheim, J.M. (2020). On the Molecular Mechanisms Regulating Animal Cell Size Homeostasis. Trends Genet. *36*, 360–372.
19. Chatzitheodoridou, D., D'Ario, M., Jones, I., Pineros, L., Serbanescu, D., O'Donnell, F., Cadart, C., and Swaffer, M.P. (2022). Meeting report - Cell size and growth: from single cells to the tree of life. J. Cell Sci. *135*.
20. Schmoller, K.M., Turner, J.J., Koivomagi, M., and Skotheim, J.M. (2015). Dilution of the cell cycle inhibitor Whi5 controls budding-yeast cell size. Nature *526*, 268–272.
21. Hasan, M.M., Brocca, S., Sacco, E., Spinelli, M., Papaleo, E., Lambrughi, M., Alberghina, L., and Vanoni, M. (2013). A comparative study of Whi5 and retinoblastoma proteins: from sequence and structure analysis to intracellular networks. Front. Physiol. *4*, 315.
22. Pappireddi, N., Martin, L., and Wuhr, M. (2019). A Review on Quantitative Multiplexed Proteomics. Chembiochem *20*, 1210–1224.
23. Liu, D., Yang, S., Kavdia, K., Sifford, J.M., Wu, Z., Xie, B., Wang, Z., Pagala, V.R., Wang, H., Yu, K., et al. (2021). Deep Profiling of Microgram-Scale Proteome by Tandem Mass Tag Mass Spectrometry. J. Proteome Res. *20*, 337–345.
24. Grabner, G.F., Xie, H., Schweiger, M., and Zechner, R. (2021). Lipolysis: cellular mechanisms for lipid mobilization from fat stores. Nat. Metab. *3*, 1445–1465.
25. Agarwal, A.K., Tunison, K., Dalal, J.S., Yen, C.L., Farese, R.V., Jr., Horton, J.D., and Garg, A. (2016). Mogat1 deletion does not ameliorate hepatic steatosis in lipodystrophic (Agpat2-/-) or obese (ob/ob) mice. J. Lipid Res. *57*, 616–630.
26. Mtaweh, H., Tuira, L., Floh, A.A., and Parshuram, C.S. (2018). Indirect Calorimetry: History, Technology, and Application. Front Pediatr *6*, 257.
27. Speakman, J.R. (2013). Measuring energy metabolism in the mouse - theoretical, practical, and analytical considerations. Front. Physiol. *4*, 34.
28. Hill, J.O., Wyatt, H.R., and Peters, J.C. (2013). The Importance of Energy Balance. Eur. Endocrinol. *9*, 111–115.
29. Mukherjee, S., and Ghosh, A. (2020). Molecular mechanism of mitochondrial respiratory chain assembly and its relation to mitochondrial diseases. Mitochondrion *53*, 1–20.
30. Chandel, N.S. (2021). Mitochondria. Cold Spring Harb Perspect Biol. *13*.
31. Roesler, A., and Kazak, L. (2020). UCP1-independent thermogenesis. Biochem. J. *477*, 709–725.
32. Cortes, V.A., Cautivo, K.M., Rong, S., Garg, A., Horton, J.D., and Agarwal, A.K. (2014). Leptin ameliorates insulin resistance and hepatic steatosis in Agpat2-/- lipodystrophic mice independent of hepatocyte leptin receptors. J. Lipid Res. *55*, 276–288.
33. Schneiter, R., Brugger, B., Sandhoff, R., Zellnig, G., Leber, A., Lampl, M., Athenstaedt, K., Hrastnik, C., Eder, S., Daum, G., et al. (1999). Electrospray ionization tandem mass spectrometry (ESI-MS/MS) analysis of the lipid molecular species composition of yeast subcellular membranes reveals acyl chain-based sorting/remodeling of distinct molecular species en route to the plasma membrane. J. Cell Biol. *146*, 741–754.
34. Kim, S.C., and Wang, X. (2020). Phosphatidic acid: an emerging versatile class of cellular mediators. Essays Biochem. *64*, 533–546.
35. Yen, C.L., Cheong, M.L., Grueter, C., Zhou, P., Moriwaki, J., Wong, J.S., Hubbard, B., Marmor, S., and Farese, R.V., Jr. (2009). Deficiency of the intestinal enzyme acyl CoA:monoacylglycerol acyltransferase-2 protects mice from metabolic disorders induced by high-fat feeding. Nat. Med. *15*, 442–446.
36. Nelson, D.W., Gao, Y., Yen, M.I., and Yen, C.L. (2014). Intestine-specific deletion of acyl-CoA:monoacylglycerol acyltransferase (MGAT) 2 protects mice from diet-induced obesity and glucose intolerance. J. Biol. Chem. *289*, 17338–17349.
37. McFie, P.J., Patel, A., and Stone, S.J. (2022). The monoacylglycerol acyltransferase pathway contributes to triacylglycerol synthesis in HepG2 cells. Sci. Rep. *12*, 4943.
38. Agarwal, A.K., Sukumaran, S., Cortes, V.A., Tunison, K., Mizrachi, D., Sankella, S., Gerard, R.D., Horton, J.D., and Garg, A. (2011). Human 1-acylglycerol-3-phosphate O-acyltransferase isoforms 1 and 2: biochemical characterization and inability to rescue hepatic steatosis in Agpat2(-/-) gene lipodystrophic mice. J. Biol. Chem. *286*, 37676–37691.
39. Mina, A.I., LeClair, R.A., LeClair, K.B., Cohen, D.E., Lantier, L., and Banks, A.S. (2018).

CalR: A Web-Based Analysis Tool for Indirect Calorimetry Experiments. Cell Metab *28*, 656–666.e651.

40. Sankella, S., Garg, A., and Agarwal, A.K. (2017). Activation of Sphingolipid Pathway in the Livers of Lipodystrophic Agpat2(-/-) Mice. J Endocr Soc *1*, 980–993.
41. Agarwal, A.K., Tunison, K., Mitsche, M.A., McDonald, J.G., and Garg, A. (2019). Insights into lipid accumulation in skeletal muscle in dysferlin-deficient mice. J. Lipid Res. *60*, 2057–2073.
42. Bligh, E.G., and Dyer, W.J. (1959). A rapid method of total lipid extraction and purification. Can. J. Biochem. Physiol. *37*, 911–917.

STAR★METHODS

KEY RESOURCES TABLE

REAGENT or RESOURCE	SOURCE	IDENTIFIER
Antibodies		
AGPAT2	Genway Biotech (custom made)	PMID: 21873652
Biological samples		
Adipose tissue depots, liver, and plasma	This study	N/A
Chemicals, peptides, and recombinant proteins		
RNA Stat-60	Fisher Scientific	Cat# nc9489785
cOmplete™ mini protease inhibitor tablets	Roche	Cat# 11836153001
Sybr Green	Thermo Fisher	Cat# 4364346
SPLASH Lipidomix standards	Avanti	Cat# 330707-1EA
Critical commercial assays		
RNeasy lipid mini extraction kit	Qiagen	Cat# 74804
DC Protein Assay Reagents Package	Bio-Rad	Cat# 5000116
Triglyceride Colorimetric Assay Kit	Cayman Chemical	Cat# 10010303
DNA-free™ DNA Removal Kit	Fisher Scientific	Cat# am1906
Reverse Transcription Reagents kit	Fisher Scientific	Cat# N8080234
Mouse Leptin ELISA Kit	Crystall Chem	Cat# 90030
TMT10plex Isobaric Mass Tagging Kit	Thermo Scientific	Cat# 90113
Pierce High pH Reversed-Phase Peptide Fractionation Kit	Thermo Scientific	Cat # 84868
Vitros 250 analyzer glucose slide	Ortho Clinical Diagnostics	Cat # 1707801
Vitros 250 analyzer triglyceride slide	Ortho Clinical Diagnostics	Cat # 1336544
Vitros 250 analyzer AST slide	Ortho Clinical Diagnostics	Cat # 8433815
Experimental models: Organisms/strains		
Mouse: Agpat2$^{-/-}$	In house	PMID 19187773
Mouse: rtTA-adiponectin	In house	PMID 22451920
Mouse: Tg-AT-hA2; mA2$^{+/+}$	This paper	N/A
Mouse: Tg-AT-hA2; mA2$^{-/-}$	In house	PMID 37752957
Oligonucleotides		
A full list of qPCR primers, see Table S3	This paper	N/A
Primer manufacturer	Integrated DNA Technologies	Coralville, IA
Primer manufacturer	Realtimeprimers.com	Elkin Park, PA
Recombinant DNA		
pBluescript-TRE-Tight	In house	PMID 22451920
Software and algorithms		
GraphPad Prism version 9.2.0	GraphPad Software	https://www.graphpad.com
FIJI (ImageJ version 1.52p)	NIH	https://fiji.sc/
BZ-X Analyzer version 1.4.1.1	Keyence	https://www.keyence.com/landing/microscope/lp_fluorescence.jsp
SAS version 9.4	SAS institute	https://www.sas.com
CalR Version 1.3	Harvard Digestive Diseases Center	https://calrapp.org/
MultiQuant	Sciex	https://sciex.com/products/software/multiquant-software
Proteome Discoverer v.3.0 SP1	Thermo Scientific	https://www.thermofisher.com

(*Continued on next page*)

Continued

REAGENT or RESOURCE	SOURCE	IDENTIFIER
Other		
Doxycycline diet	Bio-Serv	Cat# S4107
Normal chow diet	Envigo	Cat# 2916
Keyence BZ-X710 (Microscope for imaging)	Keyence	https://www.keyence.com
16 × 100 mm glass tubes with PTFE-lined caps	Fisher Scientific	Cat# 14-962-26F
Solvent-resistant plasticware pipette tips	Mettler-Toledo	Cat# 30389164
2.0 mL prefilled Bead Ruptor tube (2.8 mm ceramic beads)	Omni International	19–628
SCIEX QTRAP 6500+ LC-MS/MS	SCIEX	https://sciex.com/products/mass-spectrometers/qtrap-systems/qtrap-6500plus-system
Shimadzu LC-30AD HPLC system	Shimadzu	https://ssi.shimadzu.com/products/liquid-chromatography/index.html
150 × 2.1 mm, 5 µm Supelco Ascentis silica column	Supelco	Cat# 581509-U
Zirconium oxide beads 1.0 mm diameter	Next Advance	Cat # ZrOB10
Bruker Minispec mq10 (NMR)	Bruker Corporation	Billerica, MA
StepOne Plus Real-Time PCR System	Thermo Fisher Scientific	Waltham, MA
Bead Ruptor	Omni International	Kennesaw, GA
Mouse Genome Scanning Panel	Taconic Biosciences	GENMON-SCANSNP-M
Thermo Orbitrap Eclipse MS system coupled to an Ultimate 3000 RSLC-Nano liquid chromatography system	Thermo Fisher Scientific	https://www.thermofisher.com/order/catalog/product/FSN04-10000

RESOURCE AVAILABILITY

Lead contact

Further information and requests for resources and reagents should be directed to and will be fulfilled by the lead contact, Anil Agarwal (anil.agarwal@utsouthwestern.edu).

Materials availability

Unique materials and reagents generated in this study are available upon request from the lead contact with a completed Material Transfer Agreement.

Data and code availability

(1) All data reported in this paper will be shared by the lead contact upon request.
(2) This paper does not report original code.
(3) Any additional information required to reanalyze the data reported in this paper is available from the lead contact upon request.

EXPERIMENTAL MODEL AND STUDY PARTICIPANT DETAILS

Mouse littermates of the same sex were randomly assigned to experimental groups. All animals used in the current study are either 12 or 24 weeks of age of both sexes. All animal studies were approved by the Institutional Use and Care of Animals Committee (IUCAC) at the University of Texas Southwestern Medical Center. All methods were performed in accordance with the relevant guidelines and regulations. All animals were kept in 12-h light/dark cycles at 22°C temperature. Mice were fed either standard chow diet or doxycycline diet, as indicated in the text.

The generation of Tg-$^{AT\text{-}hA2}$;*mA2*$^{+/+}$ mice[4] described before and briefly below. The B6/129F1 mouse line was obtained from Taconic Bioscience.

Brief description of generation of Tg-$^{AT\text{-}hA2}$;*mA2*$^{+/+}$ mice

Generation of transgenic AGPAT2 mouse model

A detailed description of mouse generation was published recently.[4] To generate Tg-TRE-h*AGPAT2*, the human *AGPAT2* open reading frame (NM_006412) was amplified with the following primers, including a Kozak sequence on the forward primer and XbaI restriction sites (underlined) on both primers for ease of cloning: Forward – 5′ GCTCTAGAGCCGCCACCATGGAGCTGTGGCCGTG and Reverse – 5′ GCTCTAGATCTACTGGGCCGGCTGCAC. The amplified product was cloned into pDrive, then digested with XbaI to release the fragment.

The fragment was then cloned in XbaI restricted pBluescript-TRE-Tight vector and h*AGPAT2* was Sanger sequenced to verify no PCR error occurred.

The strategy of linearizing this plasmid for injection with the recommended NaeI and SacII restriction sites was unusable because both sites are present in our h*AGPAT2* sequence. To overcome this difficulty, we designed primers to span the NaeI and SacII restriction sites of pBluescript-TRE-Tight-h*AGPAT2,* which were flanked by SpeI restriction sites (underlined). SpeI restriction sites are not present in the h*AGPAT2* sequence. Forward – 5′ GGACTAGTAGGGAAGAAAGCGAAAGGAG; Reverse – 5′ GGACTAGTCTAAAGGGAACAAAAGCTGGA.

The fragment was digested with SpeI and ligated into the same site into a vector of convenience for Sanger sequencing and amplification. Once the correct sequence was confirmed, the fragment was excised using SpeI, purified, and provided to the transgenic core. The linearized plasmid was microinjected into C57BL/6J fertilized eggs.

Since we wanted to express hAGPAT2 only in adipose tissue, we crossed 6 male Tg-TRE-h*AGPAT2* mice with the Tg-*Adipo*-rtTA mouse line (obtained from P.E. Scherer's lab). The cross between these two lines produced a mouse strain expressing both h*AGPAT2* and rtTA protein (Tg-h*AGPAT2, Adipo*-rtTA). This mouse line, when fed doxycycline, will activate the expression of *AGPAT2* in adipose tissue.

To determine that these mice express h*AGPAT2*, we crossed six mice and their progeny were genotyped for the presence of h*AGPAT2* and *rtTA*. Those mice that were positive for both transgenes were fed doxycycline (600 mg/kg) when they were 5–6 weeks old; the pellets were changed every alternate day for 2 weeks.

The expression of hAGPAT2 protein was further confirmed by immunoblot (Figure S1C). It is to be noted that the antibody raised against human AGPAT2[38] does not recognize mouse AGPAT2 protein (in-house experience). The immunoblot shows the presence of expressed human AGPAT2 in BAT and gonadal adipose tissue.

Generation of hAGPAT2 expression in mAgpat2$^{+/+}$ background

Upon confirming the expression of *AGPAT2* regulated by doxycycline, the Tg-h*AGPAT2, Adipo*-rtTA mice were crossed with m*Agpat2*$^{+/-}$ mice to generate Tg-h*AGPAT2, Adipo*-rtTA, m*Agpat2*$^{+/-}$ mice. The Tg-h*AGPAT2, Adipo*-rtTA, m*Agpat2*$^{+/-}$ mice were genotyped and these Tg-h*AGPAT2, Adipo*-rtTA, m*Agpat2*$^{+/-}$ heterozygous mice were crossed to generate Tg-h*AGPAT2, Adipo*-rtTA, m*Agpat2*$^{+/+}$ mice. Tg-h*AGPAT2, Adipo*-rtTA, m*Agpat2*$^{+/+}$ mice were used for subsequent experiments. The mating strategy to obtain experimental animals is shown in Figure S1D. This mouse strain is abbreviated hereafter as **Tg-$^{AT\text{-}hA2}$;*mA2*$^{+/+}$**

Mouse genotyping

For genotyping of **Tg-$^{AT\text{-}hA2}$;*mA2*$^{+/+}$** mice, we used primers to amplify the Tg-TRE-h*AGPAT2,* Tg-*Adipo*-rtTA, and m*Agpat2* alleles individually: Tg-TRE-h*AGPAT2:* forward 5′ – ATGGAGCTGTGGCCGTGTCT – 3′, reverse 5′ – AGTACTTGAAGCTTCGCACG – 3′, with a product size of 217 bp. Tg-*Adipo*-rtTA: Forward 5′ – GAACAACGCCAAGTCATTCCGCTG – 3′, reverse 5′ – CTCCTGTTCCTCCAATACGCAGCC – 3′ with a product size of 212 bp. Both the amplification products were confirmed by Sanger sequencing. *Agpat2*$^{+/+}$ mice used in this study have been described.[3] Mice were genotyped using the following allele discriminating primer sets: A15, CGG CTA GGT AAG CAG TTT GA; A8, AAA GCT GTG CCA GGG TGG GT; and S175, GAT TGG GAA GAC AAT AGC AGG CAT GC. Genomic DNA amplified with A15 + A8 will produce the WT allele of 733 bp and A8+S175 will produce the knockout allele of 614 bp.

Mouse genetic background testing

The genetic background of the generated **Tg-$^{AT\text{-}hA2}$;*mA2*$^{+/+}$** mice and of B6/129 was tested using Mouse Genome Scanning panel based on ~1113 SNPs (curated by Taconic) and selected specifically to highlight differences between inbred mouse strains. **Tg-$^{AT\text{-}hA2}$;*mA2*$^{+/+}$** is a mixed genetic background of ~89% C57BL/6NTac and ~11% 129S6/SvEvTac. B6/129 mice used to ascertain the effect of doxycycline diet are also on a mixed genetic background (~50% C57BL/6NTac and ~50% 129S6/SvEvTac). B6/129 mice have been used primarily as a control for studies involving the use of targeted gene deletion/mutation. While not genetically identical to these mixed background targeted deletion/mutation mouse models, they approximate, in a consistent manner, the genetic mix that may be present in such models (https://www.taconic.com/mouse-model/b6129f1). Taconic Biosciences conducted the mouse genetic background analysis.

Oral glucose tolerance test (OGTT)

OGTT was performed in mice fasted for 6 h and then orally gavaged with D-glucose (2 g/kg body weight). Blood glucose (tail vein) was determined using a ReliOn blood glucometer (Walmart) immediately before the glucose gavage and at various time points after the administration of the glucose. Approximately 40 μL blood was collected from the tail vein in Microvette tubes (Sarstedt, Nümbrecht, Germany) containing clot activator. Tubes were spun at 10,000 g for 5 min and serum was collected for insulin measurement. Serum insulin was measured by ELISA method (Crystal Chem, Downers Grove, IL).

Indirect calorimetry

For indirect calorimetry, individual mice were placed in metabolic cages and acclimated for 72 h before the start of the experiments. The TSE LabMaster (TSE Systems GmbH, Germany) was used to collect data. Oxygen consumption (VO_2), carbon dioxide production (VCO_2), and total fluid and food intake were collected continuously over a 132 h period. The data were processed using CalR software developed by Amir I Mina and colleagues.[39]

Plasma metabolite measurements

Plasma triglyceride, glucose, and aspartate aminotransferase (AST) were measured using Dry-slide technology (Vitros 250 analyzer from Ortho Clinical Diagnostic). All measurements were carried out at the Mouse Metabolic Phenotyping Core at University of Texas Southwestern Medical Center.

Total RNA isolation

A general method routinely used by us for total RNA extraction and RT-qPCR has been described.[40] Briefly, total RNA was extracted from mouse liver tissues (~50–100 mg) using RNA STAT-60. Total RNA from adipose tissue depots was extracted using RNeasy Lipid Tissue Kit according to the manufacture's protocol. RT-qPCR was carried out and analyzed as described below.

Reverse transcription quantitative polymerase chain reaction (RT-qPCR)

Total RNA, in equal quantity, was pooled from 2 to 6 samples of either liver or adipose tissue of each genotype and sex, and RT-qPCR was carried out in a 20 μL reaction volume. A total of 1–20 μg RNA was DNase I treated using the DNase-free kit from Ambion. Complementary DNA was made using 1–2 μg DNase I-treated RNA using reverse-transcription kit from ABI. RT-qPCR was performed in duplicate using 2.5 mM primers, 20 ng complementary DNA, and SYBR Green. All RT-qPCR were carried out in 96-well plates using the StepOnePlus real-time PCR system. RT-qPCR was performed twice for liver samples and once for adipose tissue samples and in duplicate, and the transcript levels were normalized to *cyclophilin (cyclo)*. The ΔC_t value for each sample was calculated as ΔC_t = [C_t (gene of interest)-C_t (*cyclo*)]. The $\Delta\Delta C_t$ value for each gene of interest was calculated as $\Delta\Delta C_t$ = [ΔC_t (sample of interest) - ΔC_t (WT)]. The fold change was calculated as fold change = $2^{-\Delta\Delta Ct}$. Primers used for gene amplification were obtained from Harvard primer bank or were designed in-house and synthesized by Integrated DNA Technologies, or were obtained from realtimeprimers.com. Primers used in this study are provided in Table S3.

Quantitative PCR using pooled sample strategy

In a preliminary study, we amplified the expression of mRNA for several genes individually and in pooled samples and compared the raw C_t values for each gene. There is excellent correlation between the mean of individual samples to those when the samples are pooled.[41] We now routinely pool the samples for measurements of mRNA expression.[40] Furthermore, in the current study, in order to account for the experimental variance, we generated cDNA from the pooled samples two different times and amplified independently in duplicates.

Triacylglycerol assay

Liver and adipose tissue triacylglycerol (TAG) was measured using a triglyceride colorimetric assay kit from Cayman chemical according to the manufacturer's protocol with a few minor adjustments. A known quantity of liver tissue (100 mg) and 25–50 mg adipose tissue was weighed and homogenized in 1 mL of the buffer with protease inhibitor (Roche). The tissue homogenate was first spun for (3000 x g for 10 min) to break the excessive froth and transferred to a microfuge tube and spun again at 10,000 x g for 10 min. The supernatant was transferred to another tube, including the fat layer, and the volume noted. A preliminary dilution of the samples allowed us to determine the dilution appropriate to be within the range of the standard. The TAG is expressed as mg/g tissue.

Magnetic resonance imaging and spectrometry

The whole body ^{1}H NMR spectra were collected on a Varian 4.7T horizontal image scanner using a ^{13}C-^{1}H linear coil (Varian, diameter 63 mm, length 115 mm). The fat contents were analyzed as the integral of the 1.3 ppm signal relative to the total integral of both 4.7 ppm signal (water) and the 1.3 ppm signal. T1-weighted images were collected on the same machine using either a ^{1}H Litz coil (Dorty, diameter 40 mm, length 50 mm) for axial images or a ^{13}C-^{1}H linear coil (Varian, diameter 63 mm, length 115 mm) for axial, sagittal, and coronal images. The MRI parameters were TR = 580 ms, TE = 12ms, resolution 0.078 × 0.078 × 3 mm (axial) or 0.136 × 0.136 × 3 mm (coronal and sagittal). These images were obtained using 1.5 Tesla magnet and the animals were killed by cervical dislocation and all images were acquired within 30 min.

Nuclear magnetic resonance

Nuclear Magnetic Resonance (NMR) measurements of mice were obtained on the Bruker Minispec using the default parameters.

Lipid mass spectrometry

All solvents used were either HPLC or LC/MS grade and purchased from Sigma-Aldrich. SPLASH Lipidomix standards were purchased from Avanti. All lipid extractions were performed in 16 × 100mm glass tubes with PTFE-lined caps. Glass Pasteur pipettes and solvent-resistant plasticware pipette tips were used to minimize leaching of polymers and plasticizers.

Approximately 25–50 mg of adipose tissue (gonadal fat, subcutaneous (SubQ), and brown adipose tissue) was transferred to a 2.0 mL prefilled Bead Ruptor tube (2.8 mm ceramic beads), and 1 mL of methanol-dichloromethane (1:2; v/v) was added. The tissues were homogenized with a Bead Ruptor. The tissue homogenates were transferred to glass tubes and diluted to a final concentration of 20 mg/mL using the same solvent as above. Aliquots equivalent to 0.250 mg of homogenized tissue were transferred to fresh glass tubes for liquid-liquid extraction.

Samples were extracted using a modified method of Bligh/Dyer[42]; 3 mL of dichloromethane, methanol, and water (1:1:1 v/v/v) were added along with the sample. The mixture was vortexed and centrifuged at 2,671 x g for 5 min, resulting in two distinct liquid phases. The organic phase (lower phase) was drawn up with a Pasteur pipette and placed in a fresh glass tube and spiked with 20 μL of a 1:5 diluted Splash Lipidomix standard mixture. The samples were dried under liquid nitrogen and resuspended in 400 μL of hexane. Lipids were analyzed by LC-MS/MS using an SCIEX QTRAP 6500+ (SCIEX) equipped with a Shimadzu LC-30AD (Shimadzu) high-performance liquid chromatography (HPLC) system and a 150 × 2.1 mm, 5 μm Supelco Ascentis silica column (Supelco). Samples were injected at a flow rate of 0.3 mL/min at 2.5% solvent B (methyl *tert*-butyl ether) and 97.5% Solvent A (hexane). Solvent B was increased to 5% over 3 min and then to 60% over 6 min. Solvent B was subsequently decreased to 0% during 30 s while Solvent C, isopropanol-water (90:10 v/v) was set at 20% and increased to 40% during the following 11 min. Solvent C is increased to 44% over 6 min and then increased to 60% over 50 s. The system was held at 60% solvent C for 1 min prior to re-equilibration at 2.5% of solvent B for 5 min at a 1.2 mL/min flow rate. Solvent D [acetonitrile-water 95:5 (v/v) with 10 mM Ammonium acetate] was infused post-column at 0.03 mL/min. Column oven temperature was 25°C. Data was acquired in positive and negative ionization mode using multiple reaction monitoring (MRM). The LC-MS/MS data was analyzed using MultiQuant software (SCIEX). The identified lipid species were normalized to its corresponding internal standard.

Plasma leptin and insulin measurements

Plasma leptin and insulin were measured by ELISA method (Crystal Chem, Downers Grove, IL).

Tandem Mass Tag-mass spectrometry (TMT-MS) for adipose tissue

Sample preparation

Approximately 40–70 mg adipose tissues (SubQ, gonadal and brown) were dispensed in snap cap 2 mL tubes and 400 μL of RIPA buffer (minus the Triton X-100) containing protease inhibitor cocktail. Approximately 150 mg of Zirconium oxide beads were added to each tube and homogenized using Bullet Blender according to the manufacturer's suggested protocol for adipose tissue (Next Advance). The homogenates were centrifuged at 10,000 g for 10 min at 4°C and the layer below the fat layer was transferred to another tube. The lysates were centrifuged again at the same speed and time and supernatant was saved in a clean tube to avoid any residual fat. The volume of tissue lysates were measured and appropriate quantity of 25% Triton X-100 was added to final concentration of 1%. The lysates were kept on ice for ~45–60 min and sonicated 3 × 5 s at 35% amplitude using Sonics Vibracell with cooling, protein was measured DC assay kit and lysate was used for TMT mass spectrometry as follows.

Peptide labeling and fractionation

SDS was added to the tissue samples in RIPA buffer to bring it to a starting concentration of 3–5% SDS in 50 μL. Tris(2-carboxyethyl)phosphine (TCEP) was added to a final concentration of 20 mM and samples were incubated at 56°C for 30 min. After cooling, iodoacetamide was added to a final concentration of 20 mM and samples were incubated for 30 min at room temperature in the dark. 50 μg samples were then transferred to S-Trap micro columns and digested overnight with 2 μg of trypsin at 37°C. Following digestion, the peptide eluate was dried and reconstituted in 100 mM tetraethyl ammonium bromide (TEAB) buffer. The TMT10plex Isobaric Mass Tagging Kit was used to label the peptides, as per the manufacturer's instructions. The labeled reactions were cleaned and fractionated using Pierce High pH Reversed-Phase Peptide Fractionation Kit into 8 fractions according to the manufacturer's directions. The fractions were dried in a SpeedVac and reconstituted in a 2% acetonitrile, 0.1% TFA buffer.

Peptides mass spectrometry

Peptides were analyzed on a Thermo Orbitrap Eclipse MS system coupled to an Ultimate 3000 RSLC-Nano liquid chromatography system. Samples were injected onto a 75 μm i.d., 75-cm long EasySpray column and eluted with a gradient from 0 to 28% buffer B over 180 min at a flow rate of 250 nL/min. Buffer A contained 2% (v/v) acetonitrile (ACN) and 0.1% formic acid in water, and buffer B contained 80% (v/v) ACN, 10% (v/v) trifluoroethanol, and 0.1% formic acid in water at a flow rate of 250 nL/min. Spectra were continuously acquired in a data-dependent manner throughout the gradient, acquiring a full scan in the Orbitrap [at 120,000 resolution with a standard AGC (automatic gain control) target] followed by MS/MS scans on the most abundant ions in 2.5 s in the ion trap (turbo scan type with an intensity threshold of 5,000, CID (collisionally induced dissociation) collision energy of 35%, standard AGC target, maximum injection time of 35 m and isolation width of 0.7 m/z). Charge states from 2 to 6 were included. Dynamic exclusion was enabled with a repeat count of 1, an exclusion duration of 25 s and an exclusion mass width of ±10 ppm. Real-time search was used for selection of peaks for SPS-MS3 (synchronous precursor selection-mass spectrometry to the third-MS3) analysis, with searches performed against the mouse reviewed protein database from UniProt along with the sequence of human AGPAT2. Up to 1 missed tryptic cleavage was allowed, with carbamidomethylation (+57.0215) of cysteine and TMT reagent (+229.1629) of lysine and peptide N-termini used as static modifications and oxidation (+15.9949) of methionine used as a variable modification. MS3 data were collected for up to 10 MS2 peaks that matched to fragments from the real-time peptide search identification, in the orbitrap at a resolution of 50,000, HCD (high-energy C-trap dissociation) collision energy of 65% and a scan range of 100–500 m/z, which allows a sufficient range of reporter ions to be detected.

Protein identification

Protein identification and quantification were done using Proteome Discoverer v.3.0 SP1. Raw MS data files were analyzed against the mouse reviewed protein database from UniProt along with the sequence of human AGPAT2. Both Comet and Sequest HT with INFERYS Rescoring were used, with carbamidomethylation (+57.0215) of cysteine and TMT reagent (+229.1629) of lysine and peptide N-termini used as static modifications and oxidation (+15.9949) of methionine used as a variable modification. Reporter ion intensities were reported, with further normalization performed by using the total intensity in each channel to correct discrepancies in sample amount in each channel. The false-discovery rate (FDR) cutoff was 1% for all peptides. Extracted reporter ions were further normalized by using total intensity in each channel to correct sample amount error.

Histological analysis

Adipose tissue from 12 to 24-week-old mice were fixed in 4% paraformaldehyde for 48 h, embedded in paraffin, sectioned, and stained with hematoxylin and eosin (H&E). All images were acquired with a Keyence BZ-X710 microscope. The black balance was adjusted in BZ-X analyzer software, version 1.3.0.3. Adipocyte size and number was determined using the BZ-X analyzer software. All tissues were processed at the pathology core laboratory at the University of Texas Southwestern Medical Center in Dallas, Texas.

Statistical analysis

No statistical methods were used to predetermine sample size. No method of randomization was used to determine how mice were allocated to experimental groups. Statistical method used for each dataset is indicated for each figure in the figure legend. Statistical tests used are Student's *t* test, two-way ANOVA, Wilcoxon rank-sum test, and mixed model repeated measurements. We determined the sex interaction for each experimental dataset to ascertain if the male and female data could be combined, which could improve the statistical power/effect. On occasion, we did observe a sex interaction, but not in all experimental datasets. Since there was no consistency in the sex interaction, we are presenting the male and female data separately. All analyses were performed using SAS 9.4 (SAS Institute, Cary, NC). All statistical tests are two-sided, and $p < 0.05$ is considered as significant. *$p < 0.05$, **$p < 0.001$, ***$p < 0.0001$. Data are presented as mean $\pm$ SD.